Full text
blackwell-synergy.com

Neurokinin 1 receptor and relative abundance of the short and long isoforms in the human brain.

Caberlotto L, Hurd YL, Murdock P, Wahlin JP, Melotto S, Corsi M, Carletti R.

Department of Biology, Psychiatry CEDD, GlaxoSmithKline Medicine Research Centre, Verona, Italy. Laura.L.Caberlotto@gsk.com

Substance P exerts its various biochemical effects mainly via interactions through neurokinin-1 receptors (NK1). Recently, the NK1 receptor has attracted considerable interest for its possible role in a variety of psychiatric disorders including depression and anxiety. However, little is known regarding the anatomical distribution of NK1 in the human central nervous system (CNS). Riboprobe in situ hybridization, quantitative PCR and in vitro autoradiography were performed. Highest NK1 mRNA levels were localized in the locus coeruleus and ventral striatum, while moderate hybridization signals were observed in the cerebral cortex (most abundant in the visual cortex), hippocampus and different amygdaloid nuclei. Very low levels of the NK1 mRNA were detected in the cerebellum and thalamus. In view of the existence of a long and short isoform of the NK1 receptor, it was of interest to assess whether there was a differential distribution of the two splice variants in the human CNS and peripheral tissues. A quantitative TaqMan PCR analysis showed that the long NK1 isoform was the most prevalent throughout the human brain, while in peripheral tissues the truncated form was the most represented. 3H-Substance P autoradiography revealed a good correlation between receptor binding sites and NK1 mRNA expression throughout the brain, with the highest levels of binding in the locus coeruleus. These results provide the anatomical evidence that the NK1 receptors have a strong association with neuronal systems relevant to mood regulation and stress in the human brain, but do not suggest a region-specific role of the two isoforms in the CNS.

SpringerLink

Human chorionic gonadotrophin beta expression in malignant Barrett's oesophagus.

Couvelard A, Paraf F, Vidaud D, Dubois S, Vidaud M, Flejou JF, Degott C.

Service d'Anatomie Pathologique, Hopital Beaujon, 92118 Clichy cedex, France.
anne.couvelard@bjn.ap-hop-paris.fr

BACKGROUND: Human chorionic gonadotrophin beta (hCGbeta) is expressed in several non-trophoblastic tumours, and this is usually associated with aggressive behaviour. Little is known about hCGbeta expression in Barrett's adenocarcinoma. MATERIALS AND METHODS: We determined the hCGbeta profile in a large series of surgically resected Barrett's adenocarcinoma (a) at mRNA level using real-time quantitative reverse-transcription polymerase chain reaction analysis and (b) at protein level using immunohistochemistry with a polyclonal antibody and with a monoclonal antibody specific for free hCGbeta. We then sought links between the hCGbeta protein expression pattern and clinical and pathological parameters, including patient outcome as well as vascular endothelial growth factor (VEGF) expression. RESULTS: hCGbeta protein expression was observed in 43 of 76 (57%) Barrett's adenocarcinomas. We showed a strong correlation between hCGbeta protein abundance and CGB mRNA level. We observed a statistical link between hCGbeta protein expression and infiltrative tumour type ($P=0.023$), perineural neoplastic invasion ($P=0.007$) and VEGF protein expression ($P=0.016$). hCGbeta expression tended to be associated with a poor outcome (16% versus 36% survival 8 years after resection). CONCLUSION: Expression of hCGbeta correlates with specific infiltrative characteristics and is associated with higher VEGF expression. Both molecules may play a co-ordinated role in the development of Barrett's adenocarcinomas.

Assessment of proliferative activity in colorectal carcinomas by quantitative reverse transcriptase-polymerase chain reaction (RT-PCR).

Duchrow M, Hasemeyer S, Broll R, Bruch HP, Windhovel U.

Surgical Research Laboratory, Surgical Clinic, Medical University of Lubeck, Ratzeburger Allee 160, D-23538 Lubeck, Germany.

The monoclonal antibody Ki-67 and the isospecific monoclonal antibody MIB-1 are routinely used in oncology to assess the proliferation index of tumor cells. A more objective and sensitive method is the determination of the of Ki-67 protein-specific mRNA by quantitative reverse transcriptase-polymerase chain reaction (RT-PCR). In 25 resected colorectal adenocarcinomas of different stages and grades we determined between 0.2 and 4.4 amol ($10(-18)$ mol) Ki-67 protein-specific mRNA per microgram total RNA (median = 0.88 amol). The corresponding Ki-67 indices (expressing the percentage of Ki-67/MIB-I positive tumor cells) ranged from 41 to 81% (median = 61%). We found a good correlation between Ki-67 index and mRNA expression ($r = 0.75$), a significant correlation between both data and tumor stage (primary tumor, regional nodes, metastasis [pTNM] staging classification) ($p < 0.001$), but not between both data and tumor grade. Both Ki-67 indices ($p = 0.05$) and mRNA levels ($p = 0.014$) correlated significantly to the patients' survival. These results demonstrate that the Ki-67 protein-specific quantitative RT-PCR is a useful method for the characterization of tumor cell proliferation.

Comment in:

- Equine Vet J. 2002 Jul;34(4):326-7.

Molecular characterisation of carbohydrate digestion and absorption in equine small intestine.

Dyer J, Fernandez-Castano Merediz E, Salmon KS, Proudman CJ, Edwards GB, Shirazi-Beechey SP.

Department of Veterinary Preclinical Sciences, University of Liverpool, UK.

Dietary carbohydrates, when digested and absorbed in the small intestine of the horse, provide a substantial fraction of metabolisable energy. However, if levels in diets exceed the capacity of the equine small intestine to digest and absorb them, they reach the hindgut, cause alterations in microbial populations and the metabolite products and predispose the horse to gastrointestinal diseases. We set out to determine, at the molecular level, the mechanisms, properties and the site of expression of carbohydrate digestive and absorptive functions of the equine small intestinal brush-border membrane. We have demonstrated that the disaccharidases sucrase, lactase and maltase are expressed diversely along the length of the intestine and D-glucose is transported across the equine intestinal brush-border membrane by a high affinity, low capacity, Na+/glucose cotransporter type 1 isoform (SGLT1). The highest rate of transport is in duodenum > jejunum > ileum. We have cloned and sequenced the cDNA encoding equine SGLT1 and alignment with SGLT1 of other species indicates 85-89% homology at the nucleotide and 84-87% identity at the amino acid levels. We have shown that there is a good correlation between levels of functional SGLT1 protein and SGLT1 mRNA abundance along the length of the small intestine. This indicates that the major site of glucose absorption in horses maintained on conventional grass-based diets is in the proximal intestine, and the expression of equine intestinal SGLT1 along the proximal to distal axis of the intestine is regulated at the level of mRNA abundance. The data presented in this paper are the first to provide information on the capacity of the equine intestine to digest and absorb soluble carbohydrates and has implications for a better feed management, pharmaceutical intervention and for dietary supplementation in horses following intestinal resection.

Comment in:

FREE full text article at
www.bloodjournal.org

Transcript profiling of human platelets using microarray and serial analysis of gene expression.

Gnatenko DV, Dunn JJ, McCorkle SR, Weissmann D, Perrotta PL, Bahou WF.

Department of Medicine, Program in Genetics, State University of New York, Stony Brook 11794-8151, USA.

Human platelets are anucleate blood cells that retain cytoplasmic mRNA and maintain functionally intact protein translational capabilities. We have adapted complementary techniques of microarray and serial analysis of gene expression (SAGE) for genetic profiling of highly purified human blood platelets. Microarray analysis using the Affymetrix HG-U95Av2 approximately 12 600-probe set maximally identified the expression of 2147 (range, 13%-17%) platelet-expressed transcripts, with approximately 22% collectively involved in metabolism and receptor/signaling, and an overrepresentation of genes with unassigned function (32%). In contrast, a modified SAGE protocol using the Type IIS restriction enzyme MmeI (generating 21-base pair [bp] or 22-bp tags) demonstrated that 89% of tags represented mitochondrial (mt) transcripts (enriched in 16S and 12S ribosomal RNAs), presumably related to persistent mt-transcription in the absence of nuclear-derived transcripts. The frequency of non-mt SAGE tags paralleled average difference values (relative expression) for the most "abundant" transcripts as determined by microarray analysis, establishing the concordance of both techniques for platelet profiling. Quantitative reverse transcription-polymerase chain reaction (PCR) confirmed the highest frequency of mt-derived transcripts, along with the mRNAs for neurogranin (NGN, a protein kinase C substrate) and the complement lysis inhibitor clusterin among the top 5 most abundant transcripts. For confirmatory characterization, immunoblots and flow cytometric analyses were performed, establishing abundant cell-surface expression of clusterin and intracellular expression of NGN. These observations demonstrate a strong correlation between high transcript abundance and protein expression, and they establish the validity of transcript analysis as a tool for identifying novel platelet proteins that may regulate normal and pathologic platelet (and/or megakaryocyte) functions.

Transcript profiling of human platelets using microarray and serial analysis of gene expression

Dmitri V. Gnatenko, John J. Dunn, Sean R. McCorkle, David Weissmann, Peter L. Perrotta, and Wadie F. Bahou

Human platelets are anucleate blood cells that retain cytoplasmic mRNA and maintain functionally intact protein translational capabilities. We have adapted complementary techniques of microarray and serial analysis of gene expression (SAGE) for genetic profiling of highly purified human blood platelets. Microarray analysis using the Affymetrix HG-U95Av2 approximately 12 600-probe set maximally identified the expression of 2147 (range, 13%-17%) platelet-expressed transcripts, with approximately 22% collectively involved in metabolism and receptor/signaling, and an overrepresentation of genes with unassigned function (32%). In contrast, a modified SAGE protocol using the Type IIS restriction enzyme *Mmel* (generating 21–base pair [bp] or 22-bp tags) demonstrated that 89% of tags represented mitochondrial (mt) transcripts (enriched in 16S and 12S ribosomal RNAs), presumably related to persistent mt-transcription in the absence of nuclear-derived transcripts. The frequency of non-mt SAGE tags paralleled average difference values (relative expression) for the most "abundant" transcripts as determined by microarray analysis, establishing the concordance of both techniques for platelet profiling. Quantitative reverse transcription-polymerase chain reaction (PCR) confirmed the highest frequency of mt-derived transcripts, along with the mRNAs for neurogranin (NGN, a protein kinase C substrate) and the complement lysis inhibitor clusterin among the top 5 most abundant transcripts. For confirmatory characterization, immunoblots and flow cytometric analyses were performed, establishing abundant cell-surface expression of clusterin and intracellular expression of NGN. These observations demonstrate a strong correlation between high transcript abundance and protein expression, and they establish the validity of transcript analysis as a tool for identifying novel platelet proteins that may regulate normal and pathologic platelet (and/or megakaryocyte) functions. (Blood. 2003;101:2285-2293)

© 2003 by The American Society of Hematology

Introduction

Human blood platelets play critical roles in normal hemostatic processes and pathologic conditions such as thrombosis, vascular remodeling, inflammation, and wound repair. Generated as cytoplasmic buds from precursor bone marrow megakaryocytes, platelets are anucleate and lack nuclear DNA, although they retain megakaryocyte-derived mRNAs.[1,2] Platelets contain rough endoplasmic reticulum and polyribosomes, and they retain the ability for protein biosynthesis from cytoplasmic mRNA.[3] Quiescent platelets generally display minimal translational activity, although newly formed platelets such as those found in patients with immune thrombocytopenic purpura (ITP) synthesize various α-granule and membrane glycoproteins (GPs), including GPIb and GPIIb/IIIa ($\alpha_{IIb}\beta_3$). Furthermore, stimulation of quiescent platelets by agonists such as α-thrombin increases protein synthesis of various platelet proteins, including Bcl-3.[4] Like nucleated cells, the rapid translation of preexisting mRNAs may be regulated by integrin ligation to extracellular matrices.[5] In the case of platelets, the primary integrin involved in this process appears to be $\alpha_{IIb}\beta_3$ with cooperative signals mediated by the collagen receptor $\alpha_2\beta_1$.[6,7]

Integrin-mediated platelet protein synthesis appears to be regulated at the level of translation initiation involving the eukaryotic initiation factor 4E (eIF4E). Instead of directly influencing eIF4E activity via posttranslational modifications (ie, phosphorylation), platelet eIF4E activity best correlates with its spatial redistribution to the mRNA-enriched cytoskeleton.[8] Furthermore, because protein translation is partially inhibited by the immunosuppressant rapamycin, it suggests that adhesion- and/or aggregation-induced outside-in-signaling function to regulate protein synthesis through the mTOR (mammalian target of rapamycin) pathway.[6,8,9]

Despite the biologic importance of platelets and their intact protein synthetic capabilities, remarkably little is known about platelet mRNAs. Younger platelets contain larger amounts of mRNA with a greater capacity for protein synthesis, as determined by using fluorescent nucleic acid dyes such as thiazole orange.[10] This assay has been used as a quantitative determinant of younger or "reticulated" platelets (RPs). Indeed increased reticulated platelets are typically found in patients with conditions associated with rapid platelet turnover such as ITP; typically RP percentages in

such patients approach 10% to 20% of all platelets, considerably higher than in healthy control subjects.[11] Interestingly, high RPs have been associated with enhanced thrombotic risk when identified in patients with thrombocytosis,[10] suggesting that quantitatively increased mRNA levels may be associated with the prothrombotic phenotype. Whether this is related to globally altered gene expression profiles or to select changes more evident during situations of rapid platelet turnover remains unknown. Certainly, technical limitations of this assay limit its utility in defining prothrombotic genotypes,[10-12] and it cannot identify differentially expressed genes that may be causally implicated in disordered platelet phenotypes.

Toward the goal of defining the molecular anatomy of the platelet genome, we have adapted complementary techniques of microarray and serial analysis of gene expression (SAGE) for genetic profiling of highly purified human blood platelets. Microarray technology represents a "closed" profiling strategy limited by the target genes imprinted onto gene chips. In contrast, SAGE is an "open" architectural system that can be used to identify novel genes and to quantify differentially expressed mRNAs.[13-15] The sequence of each tag along with its positional location uniquely identifies the gene from which it is derived, and differentially expressed genes can be identified in a quantitative manner because the tag frequency reflects the mRNA level at the time of cellular harvest and analysis. By using both technologies, we have identified a number of previously uncharacterized genes that appear to be expressed in human platelets, while simultaneously establishing the dominant frequency of mitochondrial-expressed genomes comprising the platelet mRNA pool. These observations provide a panoramic overview of the platelet transcriptome, while additionally providing insights into the molecular pathways regulating platelet (and/or megakaryocyte) function in normal and pathologic conditions.

Materials and methods

Reagents and supplies

Thermus aquaticus (Taq) polymerase was purchased from (Roche, Indianapolis, IN). T4 DNA ligase was purchased from Invitrogen (Carlsbad, CA), and restriction enzymes were from New England Biolabs (Beverly, MA), except for *Mmel*, which was obtained from the Center for Technology Transfer (Gdansk, Poland). All oligonucleotides were synthesized on an Applied Biosystems (Foster City, CA) 3-channel synthesizer and are listed in Table 1. Monoclonal antibodies used for flow cytometric analysis included the FITC (fluorescein isothiocyanate)–conjugated anti-CD41 ($\alpha_{IIb}\beta_3$) immunoglobulin G1 (IgG1; Immunotech, Miami, FL); phycoerythrin (PE)–conjugated antiglycophorin (IgG2; Becton Dickinson Pharmingen, San Diego, CA); and peridinin chlorophyll protein (PERCP)–conjugated anti-CD45 (IgG1; Becton Dickinson Pharmingen).

Platelet isolation, purification, and immunodetection

All human subjects provided informed consent for an IRB (Institutional Review Board)–approved protocol completed in conjunction with the General Clinical Research Center at Stony Brook University Hospital. Peripheral blood (20 mL) from healthy volunteers drawn into 2 mL of 4% sodium citrate (0.4% vol/vol final concentration) was used to isolate erythrocytes by differential centrifugation (1500g) or to isolate pure leukocytes by density-gradient centrifugation as previously described.[16] Platelets collected from healthy volunteers by apheresis were used within 24 hours of collection. After addition of 2 mM EDTA (ethylenediaminetetraacetic acid), apheresis-derived platelets from a single donor were centrifuged at 140g for 15 minutes at 25°C. To minimize leukocyte contamination, only the upper 9/10 of the platelet-rich plasma (PRP) was

used for gel filtration over a BioGel A50M column (1000 mL total volume) equilibrated with HBMT (HEPES-buffered modified Tyrodes buffer: 10 mM HEPES (N-2-hydroxyethylpiperazine-N'-2-ethanesulfonic acid) pH 7.4, 150 mM NaCl, 2.5 mM KCl, 0.3 mM NaH_2PO_4, 12 mM $NaHCO_3$, 0.2% bovine serum albumen [BSA], 0.1% glucose, 2 mM EDTA). Gel-filtered platelets (GFPs) were subsequently filtered through a 5-μm nonwetting nylon filament filter (BioDesign, Carmel, NY) at 25°C and harvested by centrifugation at 1500g for 10 minutes at 25°C. Platelets were gently and thoroughly resuspended in 10 mL HBMT buffer and incubated with 120 μL murine monoclonal anti-CD45 antibody conjugated to magnetic microbeads (Miltenyi Biotec, Bergisch Gladbach, Germany) on a rotating platform for 45 minutes at 25°C. Magnetic separation columns were used to capture CD45+ cells (leukocyte fraction) by positive selection (MACS II; Miltenyi Biotec). Purified platelets were concentrated by centrifugation at 1500g and immediately used for total RNA isolation.

The efficiency of platelet purification was documented at each step by flow cytometry.[17] Briefly, aliquots containing 2×10^6 platelets were incubated with saturating concentrations of FITC-conjugated anti-CD41, PE-conjugated antiglycophorin, and PERCP-conjugated anti-CD45 for 15 minutes in the dark at 25°C, washed with phosphate-buffered saline (PBS), and fixed in PBS/1% formalin. Samples were analyzed using a FACScan (fluorescence-activated cell sorter scan) flow cytometer (Becton Dickinson) using CELLQuest software designed to quantify the number of CD45+ and glycophorin-positive events in the sample (expressed as the number of events per 100 000 CD41+ events). For some experiments, fixed platelets were permeabilized with 0.1% Triton-X/PBS for 30 minutes at 25°C prior to the addition of primary antibodies, all as previously described.[17]

Platelet protein detection was completed by sodium dodecyl sulfate (SDS)–polyacrylamide gel electrophoresis (PAGE) and immunoblot analysis as previously described, using the species-specific horseradish peroxidase-conjugated secondary antibody and enhanced chemiluminescence.[16] Antibodies included the anticlusterin monoclonal antibody (Quidel, Santa Clara, CA; 1:1000 primary and 1:10 000 secondary) and the antineurogranin rabbit polyclonal antibody (Chemicon International, Temecula, CA; 1:1000 primary and 1:10 000 secondary).

Molecular analyses and microarray profiling

Purified, individual cell fractions were resuspended in 10 mL Trizol reagent (Invitrogen), transferred into diethylpyrocarbonate (DEPC)–treated Corex (Springfield, MA) tubes, and serially purified and precipitated by using isopropanol essentially as previously described.[16] Total cellular RNA was harvested by centrifugation at 12 500g for 20 minutes at 4°C, washed 2 times with 75% ethanol (10 mL/tube), and resuspended in 100 μL DEPC-treated water. Platelet mRNA quantitation was performed by using fluorescence-based real-time PCR (polymerase chain reaction) technology (TaqMan Real-Time PCR; Applied Biosystems, Foster City, CA). Oligonucleotide primer pairs were generated by using Primer3 software (www-genome.wi.mit.edu), designed to generate approximately 200–base pair (bp) PCR products at the same annealing temperature, and are outlined in Table 1. Purified platelet mRNA (4 μg) was used for first-strand cDNA synthesis using oligo(dT) and SuperScript II reverse transcriptase (Invitrogen). For real-time reverse transcription (RT)–PCR analysis, the RT reaction was equally divided among primer pairs and used in a 40-cycle PCR reaction for each target gene by using the following cycle: 94°C for 30 seconds, 55°C for 30 seconds, 72°C for 1 minute, and 71°C for 10 seconds (40 cycles total). mRNA levels were quantified by monitoring real-time fluorometric intensity of SYBR green 1. Relative mRNA abundance was determined from triplicate assays performed in parallel for each primer pair and was calculated by using the comparative threshold cycle number (Δ-Ct method) as previously described.[18]

Gene expression profiles were completed by using the approximately 12 600-probe set HG-U95Av2 gene chip (Affymetrix, Santa Clara, CA). Total cellular RNA (5 μg) was used for cDNA synthesis by using SuperScript Choice system (Life Technologies, Rockville, MD) and an oligo(dT) primer containing the T7 polymerase recognition sequence (Primer S1; Table 1), followed by cDNA purification using GFX spin columns. In vitro transcription was completed in the presence of biotinylated ribonucleotides by using a BioArray HighYield RNA Transcript

Table 1. Oligonucleotide primers

Primer	Gene and primer direction	Sequence (5' - 3')	Nucleotide Position
S1	Oligo (dT)	5'-Bn-GGCCAGTGAATTGTAATACGACTCACTATAGGGAGGCGG- (dT)₂₄-3' →	—
Cassette A	SAGE	5'-TTTGGATTTGCTGGTCGAGTACAACTAGGCTTAATCCGACATG-3'	—
		3'-*CCTAAACGACCAGCTCATGTTGATCCGAATAAGGCTp-5'	
Cassette B	SAGE	5'-pTTCATGGCGGAGACGTCCGCCACTAGTGTCGCAACTGACTA*-3'	—
		3'-NNAAGTACCGCCTCTGCAGGCGGTGATCACAGCGTTGACTGAT-5' ←	
S2	SAGE	5'-Bn-GGATTTGCTGGTCGAGTACA-3'	—
S3	SAGE	5'-Bn-TAGTCAGGTGCGACACTAGTGGC-3'	—
GP4	Glycoprotein IIB [F]	5'-AGGGCTTTGAGAGACTCATCTGTA-3'	2094-2117
GP5	Glycoprotein IIB [R]	5'-ACAATCTTGCTGTTTGGATTCTG-3'	2301-2279
GP6	Glycoprotein IIIA [F]	5'-TATAAAGAGGCCACGTCTACCTTC-3'	2335-2358
GP7	Glycoprotein IIIA [R]	5'-CACTTCCACATACTGACATTCTCC-3'	2532-2509
PAR18	PAR1 [F]	5'-AATGTCAGTTCTGATATGGAAGCA-3'	2585-2608
PAR19	PAR1 [R]	5'-CCCAAATGTTCAAACTTCTTTAGC-3'	2776-2753
SR8	16S rRNA [F]	5'-TGCAAAGGTAGCATAATCACTTGT-3'	2586-2609
SR9	16S rRNA [R]	5'-GTTTAGGACCTGTGGGTTTGTTAG-3'	2785-2762
NADH10	NADH2 [F]	5'-CTAGCCCCCATCTCAAATCATATAC-3'	4875-4898
NADH11	NADH2 [R]	5'-AATGGTTATGTTAGGGTTGTACGG-3'	5075-5052
THYM12	Thymosin β4 [F]	5'-AAGACAGAGACGCAAGAGAAAAAT-3'	135-158
THYM13	Thymosin β4 [R]	5'-GCAGCACAGTCATTTAAACTTGAT-3'	336-313
CLUS14	Clusterin [F]	5'-CCAACAGAATTCATACGAGAAGG-3'	1006-1028
CLUS15	Clusterin [R]	5'-CGTTATATTTCCTGGTCAACCTCT-3'	1222-1199
NRG16	Neurogranin [F]	5'-GCCCTTTTAGTTAGTTCTGCAGTC-3'	1351-1374
NRG17	Neurogranin [R]	5'-TTTTCTTTAAGTGAGTGTGCTTGG-3'	1567-1544
TCR18	T-cell receptor β-chain [F]	5'-CCACAACTATGTTTTGGTATCGT-3'	131-153
TCR19	T-cell receptor β-chain [R]	5'-CTAGCACTGCAGATGTAGAAGCT-3'	332-310
CD4520	CD45 [F]	5'-GCTCAGAATGGACAAGTA-3'	3771-3788
CD4521	CD45 [R]	5'-CACACCCATACACACATACA-3'	4280-4261

[F] indicates forward (sense) strand; [R], reverse (antisense) strand; Bn, biotin; p, a phosphorylated 5' end (cassettes A and B); underlining, NlaIII sites in cassettes A and B; arrows, corresponding sequence for S2 and S3 within cassettes A and B, respectively; bold, the MmeI site; and N, A, C, T, or G, nucleotide position based on the following accession numbers: glycoprotein IIB (J02764), glycoprotein IIIA (M35999), PAR1 (M62424), 16S rRNA and NADH2 (NC_001807), thymosin β4 (M17733), clusterin (M25915), neurogranin (X99076), TCR β-chain (AF043182), CD45 (Y00638).

*Indicates an amino-modified 3' end in both cassettes; —, not applicable.

Labeling Kit (Enzo Diagnostics, Farmingdale, NY), and, after metal-induced fragmentation, 15 μg biotinylated cRNA was hybridized to the HG-U95Av2 oligonucleotide probe array for 16 hours at 45°C. After washing, the cRNA was detected with streptavidin-phycoerythrin (Molecular Probes, Eugene, OR) and analysis was completed by using a Hewlett-Packard Gene Array Scanner (Affymetrix). The average difference value (AD) for each probe set was quantified using MAS 4.01 software (Affymetrix), calculated as an average of fluorescence differences for perfectly matched versus single-nucleotide mismatched 25-mer oligonucleotides (16 to 20 oligonucleotide pairs per probe set). The software is designed to exclude "positive calls" in the presence of high average differences with associated high mismatch intensities.

SAGE profiles

Platelet SAGE libraries were generated essentially as previously described,[15] modified as outlined in Figure 1 for the use of MmeI as the tagging enzyme.[19] This type IIS restriction enzyme cleaves 20 of 18 bp past its nonpalindromic (TCCRAC) recognition sequence, thereby generating longer tags (21- or 22-mer) than those obtained using BsmFI as the standard tagging enzyme (13-14 bp tags). These longer MmeI-generated tags potentially provide for more definitive "tag-to-gene" identification and are particularly useful in characterizing expression patterns in the absence of complete genomic sequence data (comprehensive methods detailed in Dunn et al[19]). Briefly, poly(A) mRNA was isolated from 10 μg total platelet RNA using the oligo-(dT) S1 primer conjugated to magnetic beads (Dynal Biotech, Lake Success, NY), followed by cDNA synthesis using SuperScript II reverse transcriptase (Invitrogen). The cDNA was then digested

with the restriction enzyme NlaIII (anchoring enzyme), ligated to cassette A using T4 DNA ligase, and, after the beads were extensively washed, the cDNA was digested with MmeI to release the tags from the beads. After purification, tags were ligated to degenerate cassette B linkers (specifically
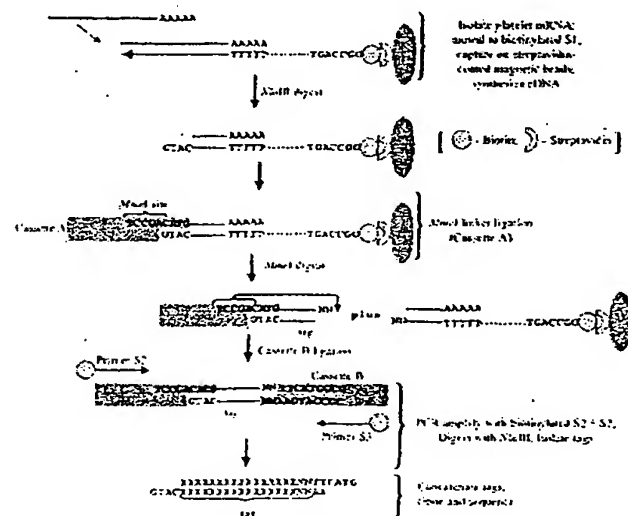

Figure 1. Schema outlining the modified SAGE protocol used in platelet analyses. The final tags are flanked by the NlaIII (anchoring enzyme) CATG sequence, thereby providing tag-to-gene identification when exported to a relational database (refer to "Bioinformatic analyses" and Table 1 for details).

designed to anneal to the nonuniform *Mme*I overhangs), and PCR-amplified using biotinylated primers S2 and S3 for 30 cycles (95°C for 30 seconds; 58°C for 30 seconds; 72°C for 30 seconds) using Platinum Taq DNA polymerase (Gibco BRL). A fraction (20%) of the pooled PCR products were then subjected to one round of linear amplification using primer pair S2/S3, followed by a second round of 25 amplifications using primer S2 alone (95°C for 30 seconds, 58°C for 30 seconds, 72°C for 30 seconds). Primer S3 was subsequently added for one cycle (95°C for 2.5 minutes, 58°C for 30 seconds, 72°C for 5 minutes); the latter steps were collectively adapted to exclude heteroduplex formation.[18] Unincorporated primers were removed by incubation with 200 U *Escherichia coli* exonuclease I for 60 minutes at 37°C. PCR products were then pooled and digested with *Nlo*III to release tags, and biotinylated linker arms were cleared using streptavidin-coated immunoaffinity magnetic beads (Dynal Biotech). Tags were con-catamerized using 5 U/μL T4 DNA ligase, and products more than 100 bp were isolated by size-fractionation in low-melting agarose gels. The DNA was purified by GFX spin columns, and the concatamers were cloned into the *Sph*I site of pZero (Invitrogen). After transformation into *E coli* TOP10 cells, recombinant clones were isolated and sequenced in 96-well microtiter plates using an ABI 377 sequencer and ABI Prism BigDye terminator chemistry (Perkin-Elmer Applied Biosystems, Branchburg, NJ).

Bioinformatic analyses

Functional grouping of genes determined to be present by Affymetrix MAS 4.01 software was performed using a dChip program linked to the National Center for Biotechnology LocusLink, which is an annotated reference database for genes and their postulated functions.[20] Of the approximately 12 600-probe sets represented on the Affymetrix HG-U95Av2 Gene chip, functional annotations exist for approximately 8100 with the remainder categorized as unknown. Microarray data were visualized and analyzed using BRB-ArrayTools software (Version 2.1), kindly developed and provided by Dr Richard Simon and Amy Peng (linus.nci.nih.gov/BRB-ArrayTools.html). A logarithmic (base 2) transformation was applied to the average difference values for individual data sets for determination of microarray concordancies. Discordancy was defined as a 2-log difference in the maximum log intensities between individual experiments.

SAGE tags were extracted by using in-house SAGE software uniquely modified to identify *Mme*I tags. The software ensures that only unambiguous 21- to 22-bp tag sequences are extracted for transcript profiling. Tags with ambiguities (Ns), lengths other than 21 or 22 bp, or with ambiguous orientations were extracted to separate files for manual editing or further examination. Finalized data were exported to a relational database for tag quantification and genetic identification.[20]

Results

Platelet purification

To ensure that the RNA profiles accurately represented those of circulating blood platelets, a number of complementary methods were implemented to remove contaminating nucleated leukocytes. Purification methods incorporating gel filtration, a 5-μm leukocyte reduction filter, and magnetic CD45 immunodepletion allowed for the cumulative enrichment of highly purified platelets. The efficacy of this purification method was initially established by using peripheral blood platelet-rich plasma as the starting material. The final product contained no more than 3 to 5 leukocytes per 1 × 10⁵ platelets as determined by parallel flow cytometric analysis, representing an approximate 450-fold reduction of nucleated leukocytes. These results correlated well with molecular evidence for leukocyte depletion as determined by RT-PCR using both CD45 and T-cell receptor β-chain (TCRβ) primers (see Figure 2). Because the total RNA yield from peripheral blood platelets was insufficient for microarray studies, we adapted the protocol to platelet apheresis donors with nearly identical final purity (Figure
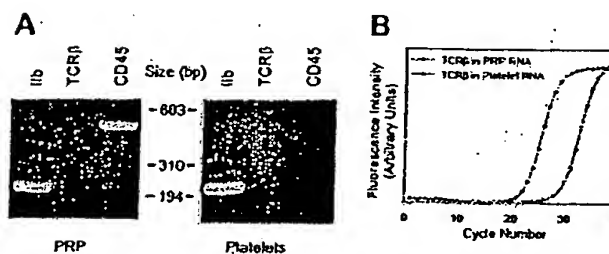

Figure 2. Determination of platelet purity. (A) Total cellular RNA (1.8 μg) from platelet-rich plasma (PRP) or purified platelets from a single apheresis donor were analyzed by RT-PCR (35 cycles) using oligonucleotide primers specific for glycoprotein IIb (GPIIb), T-cell receptor β-chain (TCRβ), or CD45; 10 μL of the 50 μL reactions were analyzed by ethidium-stained agarose gel electrophoresis. Minimal to no TCRβ gene product was visually evident only in PRP. Size markers corresponding to *Hae*III-restricted φX174 DNA are shown. (B) Real-time RT-PCR was completed by using 1.8 μg total RNA and TCRβ-specific oligonucleotide primers optimized for quantitative analysis by real-time PCR.[18] On the basis of parallel determinations using RNA isolated from known amounts of purified leukocyte standards, the leukocyte-depletion protocol represents an approximate 2.5-log purification from the starting PRP. Results are representative of one complete set of experiments repeated on 2 separate occasions, and data points represent the mean from triplicate wells, with standard errors of the mean (SEM) less than 1% (not shown).

2). The platelet recovery was nearly 65% of the starting material, yielding approximately 2.3×10^{11} platelets from an initial apheresis pack containing approximately 3.6×10^{11} platelets. The bulk of the losses occurred during the initial centrifugation and filtration steps. The purification protocol was less effective at removing erythrocytes, although there were less than 50 glycophorin-positive cells per 1×10^5 platelets after the final purification step. Nonetheless, these cells represent unlikely sources for contaminating cellular RNA (see "Cellular microarray analysis" below).

Cellular microarray analysis

The purified platelet RNA was sufficient for microarray studies and was used for cRNA generation and hybridization to the Affymetrix HG-U95Av2 GeneChip. The anatomic profile of platelet RNAs from 3 healthy male donors was determined by using Affymetrix software. Of the 12 599 probe sets imprinted onto the chip, a maximum of 2147 (17%) transcripts were computationally identified as "present" by the Affymetrix software, 152 (1.2%) were equivocal, and nearly 82% were absent. As a fraction of the total genes present on the chip, the percentage of platelet-expressed genes (15%-17%) was generally lower than that obtained from other human cell types in which 30% to 50% of genes are present as determined by Affymetrix software (J. Schwedes, personal communication, May 2002). The "limited number" of platelet-expressed transcripts presumably reflects the lack of ongoing gene transcription in the anucleate platelet. Because less than 1% of circulating red blood cells contain residual RNA, it is unlikely that any of these transcripts are erythrocyte derived, although this was formally addressed by isolating total cellular RNA from 20 mL of whole blood (corresponding to an ~3-log fold excess of erythrocytes than that identified in our final sample). The total cellular yield of RNA from this starting material was approximately 250 ng, suggesting that less than 1 ng erythrocyte-derived RNA was present in the purified platelet preparations. Despite this, however, both α- and β-globin transcripts—along with both the ferritin heavy and light chains—were identified as abundant transcripts (Table 2). Although the most parsimonious explanation would be residual contaminating reticulocytes, this is not supported by our erythrocyte contamination estimates, and their significance remains unresolved.

As a means of better dissecting the molecular anatomy of the platelet, expressed genes were grouped on the basis of assigned

Table 2. Top 50 human platelet-expressed genes

Accession no.	Gene symbol	AD values, range*	Gene transcript†	Leukocyte expression‡
M17733	TMSB4X	140 142-307 852	Thymosin β4 mRNA, complete cds	+
X99076	NRGN	101 510-148 279	Neurogranin gene	+
M25079	HBB	40 839-229 556	β-globin mRNA, complete cds	+
M25915	CLU	84 720-140 246	Complement cytolysis inhibitor (clusterin) complete cds	−
J04755	FTHP1	82 980-148 621	Ferritin H processed pseudogene, complete cds	−
D78361	OAZ1	73 098-118 140	mRNA for ornithine decarboxylase antizyme	−
X04409	GNAS	77 761-94 781	mRNA for coupling protein G(s) α-subunit (alpha-S1)	−
M25897	PF4	62 811-126 908	Platelet factor 4 mRNA, complete cds	−
AB021288	B2M	61 689-108 921	β2-microglobulin	+
X00351	ACTB	25 143-73 775	mRNA for β-actin	−
D21261	TAGLN2	76 687-101 931	mRNA for KIAA0120 gene	+
AL031670	FTLL1	69 865-99 966	Ferritin, light polypeptide 1	+
U59632	GPIIB	41 404-110 328	Platelet glycoprotein Ibβ chain mRNA	−
M21121	CCL5	47 308-106 399	T-cell-specific protein (RANTES) mRNA, complete cds	−
X13710	GPX1	41 318-96 878	Unspliced mRNA for glutathione peroxidase	−
J00153	HBA1	21 326-144 201	Alpha globin gene cluster on chromosome 16	+
M22919	MYL6	46 337-106 833	Nonmuscle/smooth muscle alkali myosin light chain gene	+
L20941	FTH1	52 787-74 763	Ferritin heavy chain mRNA, complete cds	−
J03040	SPARC	51 156-74 261	SPARC/osteonectin mRNA, complete cds	−
X56009	GNAS	45 543-72 096	GSA mRNA for α subunit of GsGTP binding protein	−
X58536	HLA	31 183-82 613	mRNA for major HLA class I locus C heavy chain	+
M54995	PPBP	46 571-67 169	Connective tissue activation peptide III mRNA	−
U34995	GAPD	35 095-70 250	Normal keratinocyte substraction library mRNA, clone H22a	+
L40399	MLM3	32 107-73 364	Clone zap112 (mutL protein homolog 3) mRNA	−
X77548	NCOA4	31 452-61 036	cDNA for RFG (RETproto-oncogene RET/PTC3)	−
U90551	H2AFL	35 086-51 892	Histone 2A-like protein (H2A/l) mRNA	−
M11353	H3F3A	31 614-55 813	H3.3 histone class C mRNA	−
Z12962	RPL41	36 003-54 853	mRNA for homologue to yeast ribosomal protein L41	+
X06956	TUBA1	20 988-61 798	HALPHA 44 gene for α-tubulin	−
AB028950	TLN1	24 571-58 611	mRNA for KIAA 1027 protein	−
Y12711	PGRMC1	33 680-43 174	mRNA for putative progesterone binding protein	−
M16279	MIC2	30 894-48 166	Integrated membrane protein (MIC2) mRNA	−
D78577	YWHAH	24 785-50 437	Brain 14-3-3 protein β-chain	−
AF070585	TOP3B	20 027-67 945	Clone 24675, unknown cDNA	−
AA524802	Unknown	23 846-39 481	CDNA, IMAGE clone 954213	−
AB009010	UBC	28 745-38 389	mRNA for polyubiquitin UbC	+
X57985	H2AFO	21 678-52 108	Genes for histones H2B.1 and H2A	−
X54304	MLCB	25 733-34 109	mRNA for myosin regulatory light chain	−
M14539	F13A1	23 691-48 474	Factor XIII subunit α-polypeptide mRNA, 3' end	−
AI540958	Unknown	24 872-41 118	cDNA, PEC 1.2_15_HOl.r 5' end /clon	−
AL050396	FLNA	13 634-55 235	cDNA DKFZp 586K1720	−
X56841	HLA-E	12 890-49 327	Nonclassical MHC class I antigen gene	−
M26252	PKM2	15 450-47 786	TCB (cytosolic thyroid hormone-binding protein)	−
M14630	PTMA	19 314-45 088	Prothymosin alpha mRNA	−
AF045229	RGS10	19 156-34 243	Regulator of G protein signaling 10 mRNA	−
AA477898	Unknown	16 863-44 756	cDNA, Z834l08.rl 5' end	−
X95404	FL1	15 216-37 456	mRNA for nonmuscle type cofilin	−
M34480	ITGA2B	8 627-45 495	Platelet glycoprotein IIb (GPIIb) mRNA	−
Z83738	H2BFE	18 001-31 306	HH2B/e gene	−
L19779	H2AFO	17 319-38 951	Histone H2A.2 mRNA, complete cds	−

*Gene expression quantifications were calculated as the average difference (AD) value (matched versus mismatched oligonucleotides) for each probe set using Affymetrix GeneChip software, version 4.01. The range of values from 3 distinct platelet microarrays is shown; the normalization value for all microarray analyses was 250.

†Transcripts are rank-ordered (highest to lowest) using BRB-ArrayTools software by log-intensities of AD values obtained from 3 different healthy donors; 33 of the top 40 transcripts were listed among the top 50 in all 3 microarray sets.

‡Leukocyte expression was determined by microarray analysis using purified peripheral blood leukocytes, followed by construction of rank-intensity plots for comparison to platelet top 50 transcripts. [20] Top leukocyte-derived transcripts identified within the ranked top 50 platelet transcripts are depicted by a (+) present, or (−) absent.

cds indicates coding sequence.

gene annotations, and this analysis was used to provide a panoramic definition of the platelet transcriptome. Of the genes that could be cataloged within assigned "clusters," those involved in metabolism (11%) and receptor/signaling (11%) represented the largest groups. Also evident in these analyses is the relatively large percentage of genes involved in functions unrelated to these key groups (ie, miscellaneous, 25%), and the overrepresentation of genes with unknown function (32%) as annotated by Affymetrix

and RefSeq databases.[21] These results identify a vast array (nearly one half) of platelet genes (and gene products) that presumably have important, but poorly characterized functions, in platelet and/or megakaryocyte biology.

Although microarray analysis is not truly quantitative, rank-ordering using the mean log-intensities from 3 independent microarray analyses allowed for the categorization of the top platelet transcripts (Table 2). Computational analyses demonstrated that

only 10 of the top 100 genes were discordant among the 3 platelet microarrays, although 71 of 100 genes were discordant between platelet and leukocyte arrays. An inventory of the top 50 platelet genes is listed in Table 2, which also delineates those found to be highly expressed in peripheral blood leukocytes by parallel microarray experiments with this purified cellular fraction (data not shown). Further analysis of these cell subsets demonstrated that approximately 25% (n = 547) of the total platelet transcripts were platelet restricted. Furthermore, only 10 of the 50 most highly expressed genes were found to overlap, confirming the distinct cellular profiles of each transcriptome. Of the 12 overlap genes, 3 corresponded to globin or ferritin chains (again suggesting the presence of contaminating reticulocytes in both purified fractions), and another 4 were involved in actin cytoskeletal reorganization and human leukocyte antigen (HLA) expression, gene products that regulate critical functions in both cell types. Given the importance of cytoskeletal reorganization in downstream platelet activation events, it is not unexpected that components of the actin machinery system would demonstrate prominent transcript expression. Previous estimates suggest that 20% to 30% of the total platelet proteome is comprised of actin with other components such as actin-binding protein, mysosin, and talin accounting for an additional 2% to 5% of the total protein.[1,22] The mRNAs encoding the actin-related machinery are overrepresented in our microarray analysis, with 8 such transcripts found among the 50 highest platelet-expressed genes. Interestingly thymosin β4 demonstrated the highest expression pattern. In unstimulated platelets, 30% to 40% of actin is polymerized as F-actin,[22] whereas the balance of actin monomers (G-actin) are polymerization inhibited by sequestering proteins such as profilin (100 μM) and thymosin β4 (600 μM).[23] The high thymosin β4 transcript expression not only correlates with its known abundance in platelets but also supports the importance of actin inhibitory proteins in maintaining the nonstimulated state of circulating platelets.

Platelet SAGE analyses

Although these initial studies identified the distribution and relative expression patterns of the genes within the Affymetrix data set, they do not allow for analyses of genes that are unrepresented by these oligonucleotide chips. Unlike closed microarray profiling strategies, SAGE is an open architectural system that is ideally suited for novel gene and pathway identification. Accordingly, the platelet RNA used for microarray studies was used for platelet SAGE. A total of 2033 tags were initially cataloged, of which 1800 (89%) corresponded to mitochondrial-derived genes. These results were quite different from those obtained by microarray analyses, but the discrepancy can be resolved by the nonrepresentation of the mitochondrial genome on the gene chip. The mitochondrial genome is a compact approximately 16.6-kilobase (kb) sequence encoding 13 genes and 2 ribosomal subunits.[24] Primary mitochondrial transcripts are polycistronic and typically contain premature termination or unpredictable splice sites, resulting in multiple polyadenylated transcripts from individual genes.[24,25] Indeed, the overall distribution of platelet-derived mitochondrial SAGE tags is quite similar to that found in muscle.[25] All 13 genes containing NlaIII sites were detected, whereas neither of the non-NlaIII-containing genes were identified (nicotinamide adenine dinucleotide [NADH] dehydrogenase subunit 4L and adenosine triphosphatase [ATPase] 8). Most of the tags were from the 16S and 12S ribosomal RNAs—which collectively accounted for 68% of the total mitochondrial tags—with the fewest tags represented by NADH dehydrogenase subunits 3, 5, 6, and cytochrome c oxidase 1
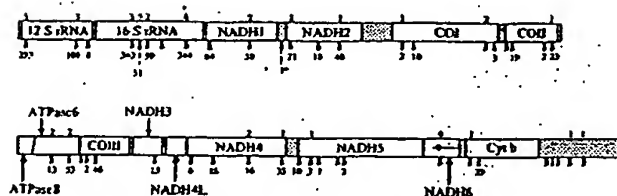

Figure 3. Schema of the mitochondrial genome with SAGE tag distributions (only tags with identical matches are displayed). The abundance of the SAGE tags (n = 1800) at individual NlaIII sites (arrows) within the mitochondrial heavy strand is shown on the bottom, whereas those tags corresponding to the mitochondrial light strand are delineated above the arrows (the presence of an unaccompanied arrow implies no SAGE tags at that NlaIII site). The gene products of mt-DNA (RefSeq accession no. NC_001807) are delineated by the open rectangles, whereas stippled boxes represent tRNA genes and control regions (the single tag represented by the [*] refers to mitochondrial transfer RNA-serine). Note that NADH6 is encoded by the light strand and that there are no NlaIII sites within the ATPase8 gene segment. CO[n], cytochrome c oxidase subunit; Cyt b, cytochrome b.

(Figure 3). The NADH dehydrogenase subunit 6 RNA is the only mRNA encoded by the light (L) strand of mitochondrial DNA and was the least abundantly detected transcript.

The unusually high preponderance of mitochondrial-derived genes is not inconsistent with the known enrichment of these genomes in human platelets,[1,24] and presumably reflects persistent transcription from the mitochondrial (mt) genome in the absence of nuclear-derived transcripts. This overrepresentation of mtDNA in platelets is considerably greater than that of its closest cell type (skeletal muscle), in which mt genomes represent approximately 20% to 25% of all SAGE tags.[25] Interestingly, the energy metabolism of platelets is not dissimilar from that of skeletal muscle, both cell types actively using glycolysis and large amounts of glycogen for ATP generation.[26] Like muscle, platelets are metabolically adapted to rapidly expend large amounts of energy required for aggregation, granule release, and clot retraction. Similar to the situation in all eukaryotic cells, platelet mitochondria represent the primary source of ATP, which is generated from oxidative phosphorylation reactions occurring within these organelles. Mitochondria are also responsible for most of the toxic reactive oxygen species generated as by-products of oxidative phosphorylation and are central regulators of the apoptotic process in other cellular types. The mtDNA encodes polypeptides found within 4 of the 5 multifunctional complexes that regulate oxidative phosphorylation within the platelet mitochondria.[27] Whether the continued generation of these polypeptides has a role in platelet energy metabolism and/or the apoptotic mechanisms regulating platelet survival remains speculative, although not inconsistent with our observations.

Comparative analysis of SAGE and microarray transcript abundance

Complete SAGE libraries require the sequencing of up to 30 000 tags for an exhaustive cataloging of individual mRNAs, especially those with limited copy numbers.[13,28] Given the preponderance of mt-derived transcripts, comparable sampling would have required sequence analysis of nearly 300 000 SAGE tags, an inordinate number for comprehensive analysis of the platelet transcriptome. For platelets, alternative methodologies incorporating subtractive SAGE will be required for more comprehensive transcript profiling.[29] Our initial sampling of nonmitochondrial genes remains informative, however, and entirely consistent with the results of platelet microarray studies. As shown in Table 3, SAGE tags for the genes encoding thymosin β4, β2-microglobulin, neurogranin, and the platelet glycoprotein Ibβ polypeptide were among the most frequently identified platelet genes, similar to the rank-ordered results determined by microarray analysis. To formally confirm the

Table 3. SAGE-identified nonmitochondrial tags

Frequency	CATG + SAGE tags*	Accession no.†	Gene	Microarray‡
26	GTTGTGGTTAATCTGGT	NM_004048.1	β2-microglobulin (B2M), mRNA	PPP
21	TTGGTGAAGGAAGAAGT	NM_021109.1	Thymosin β4, X chromosome (TMSB4X), mRNA	P
8	AGCTCCGCAGCCAGGTC	NM_002620.1	Platelet factor 4 variant 1 (PF4V1), mRNA	p
8	AGCTCCGCAGCCGGGTT	NM_002619.1	Platelet factor 4 (PF4), mRNA	P
7	TGTATAAAGACAACCTC	NM_002704.1	Proplatelet basic protein (β-thromboglobulin)	Pp
5	GGGCACAATGCGGTCCA	NM_000407.1	Glycoprotein Ibβ polypeptide, mRNA	P
3	AGGTAATAAAAGGTAAT	NM_003512.1	H2A histone family, member L (H2AFL), mRNA	P
3	AGTGGCAAGTAAATGGC	NM_021914.2	Cofilin 2 (muscle) (CFL2), mRNA	N/A
3	TGACTGTGCTGGGTTGG	NM_006176.1	Neurogranin (protein kinase C substrate, RC3) mRNA	P
3	TTGGGGTTTCCTTTACC	NM_002032.1	Ferritin, heavy polypeptide 1 (FTH1), mRNA	P
2	CCCTTGTGACTACCTAT	NM_025158.1	Hypothetical protein FLJ22251 (FLJ22251), mRNA	N/A
2	CCTGTAACCCCAGCTAC	NM_032779.1	Hypothetical protein FLJ14397 (FLJ14397), mRNA	N/A
2	CTTGTAGTCCCAGCTAC	NM_017962.1	Hypothetical protein FLJ20825 (FLJ20825), mRNA	N/A

*Unique tags identified more than once.

†Refers to the RefSeq accession no.[21] Note that this number does not necessarily correspond to the accession no. provided by Affymetrix software annotations (Table 1).

‡Presence (P) or absence (A) is based on results from 3 distinct platelet microarray experiments. Capitalized "P" designates a gene that is in the top 50 on all 3 microarray experiments, whereas small "p" designates those transcripts not in the top 50. Two of the genes (β2-microglobulin and β-thromboglobulin) are represented by 3 and 2 probe sets, respectively, on the HG-U95Av2 gene chip; for β2-M, all 3 probe sets were in the top 50 genes, whereas for thymosin β4 1 of 2 was in the top 50 for all experiments (the other probe set was in the top 75 for all experiments). N/A indicates oligonucleotide not present on Affymetrix HG-U95Av2 gene chip.

results independently obtained by SAGE and microarray analysis, quantitative RT-PCR was completed by using oligonucleotide primers specific for 2 abundant mitochondrial transcripts, 16S rRNA and NADH2 thymosin β4 (high-abundance by microarray and SAGE), 2 incompletely characterized high-abundance transcripts (neurogranin and clusterin; see "Protein immunoanalysis of platelet clusterin and neurogranin"), a low-abundant transcript (T-cell receptor β-polypeptide), and the genes encoding proteins with well-established quantitative determinations (ie, glycoprotein $\alpha_{IIb}\beta_3$ [~50 000 receptors/platelet]; protease-activated receptor-1 (PAR1) [~1800 receptors/platelet]).[1] As shown in Figure 4, these analyses reveal excellent concordance between SAGE and microarray studies, demonstrating the predominant frequency of the mitochondrial-derived 16S rRNA/NADH2 transcripts, with incrementally lower expression of other transcripts as initially demonstrated by microarray (16S > NADH2 > thymosin β4 > neurogranin > clusterin > $\alpha_{IIb}\beta_3$ > PAR1 > TCRβ).

Given the small number of nonmitochondrial SAGE tags available for analysis (n = 233), limited conclusions can be drawn using traditional (nonsubtraction) platelet SAGE libraries as pre-
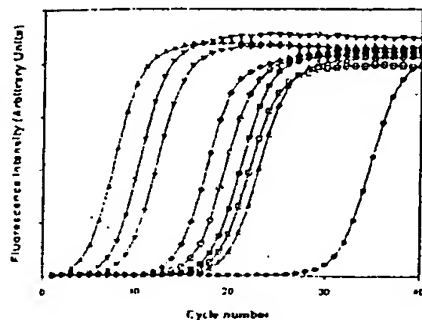

Figure 4. Quantitative real-time RT-PCR analysis of platelet transcripts. Real-time RT-PCR was completed by using purified platelet RNA and oligonucleotide primer pairs specifically designed using Primer3 software to generate similarly-sized (~200-bp) PCR products, optimized to the same annealing temperature. In graph, (□) represents IIb, (■) represents IIIa, (⊡) represents PAR1, (▲) represents 16S rRNA, (▽) represents NADH2, (▼) represents thymosin, (○) represents clusterin, (◆) represents neurogranin, and (●) represents TCRβ. Curves are representative of one complete set of experiments (repeated twice), and line plots reflect average determinations from 3 wells performed in parallel with SEM less than 1% for all data points.
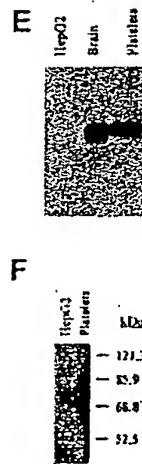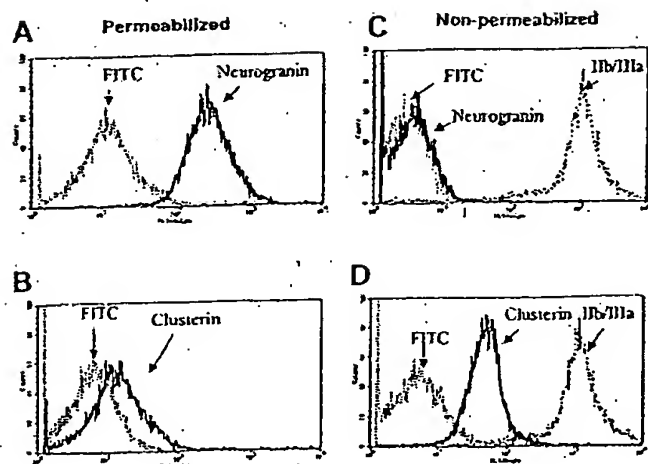
sented here. Overall, a total of 126 unique tags were identified, the majority of which (94) were represented only once. Of the total unique tags, nearly one half represented novel genes not present on the Affymetrix U95Av2 GeneChip. Of the genes with unique tags identified more than once, there was excellent concordance with microarray expression analysis, with nearly all of the SAGE tags in Table 3 corresponding to platelet top 75 microarray transcripts. The platelet factor (PF) 4 variant represents a single aberration because this was rank-ordered approximately 350 by microarray, although its SAGE tag frequency was identical to that of the predominant PF4 transcript. The lack of extensive nonmitochondrial SAGE sampling precludes any further extrapolations from this apparent aberration. Of note, a subset of these tags had long poly(A) tracts; although they all corresponded to genes identified in the RefSeq database.[21] We cannot exclude the possibility of a SAGE artifact for this small subset of tags (~2%, representing 46 of 2033 tags), although the authenticity of the vast majority of tags (~98%) clearly validates the methodology. These tags are most likely explained by the unique biology of the platelet (ie, mRNA decay in the absence of de novo transcription) or to mRNA degradation occurring during the extensive purification methods. In summary, even with a remarkably limited sampling, the power of this approach in gene identification of relatively abundant and less abundant transcripts is evident. It is clear, however, given the unique molecular anatomy of the platelet (ie, abundance of mitochondrial transcripts), that SAGE adaptations will be required for more comprehensive genetic profiling.[29]

Protein immunoanalysis of platelet clusterin and neurogranin

Although most of the "most abundant" transcripts would conform to a priori predictions for platelet-expressed mRNAs, a number of transcripts were identified that had been poorly characterized in human platelets. To further establish the authenticity of highly expressed transcripts such as clusterin and neurogranin, confirmatory protein analyses were completed. As shown in Figure 5, both proteins were clearly detected in purified platelet lysates; furthermore, their cellular platelet distributions conformed to those predicted based on previously proposed functions. Note for example that clusterin—functionally characterized as a complement lysis inhibitor able to block the terminal complement reaction—is primarily expressed on the extracellular platelet membrane.[30]

Figure 5. Immunoanalysis of platelet neurogranin and clusterin. (A-D) Gel-filtered platelets were either fixed in 3.7% formaldehyde (nonpermeabilized) or fixed with permeabilization in the presence of 0.1% Triton-X; followed by flow cytometric analysis using anticlusterin, anti-IIb/IIIa, or antineurogranin antibodies and the FITC-conjugated species-specific secondary antibody (in C, the FITC-conjugated antirabbit and antimouse controls are essentially superimposed). (E-F) Ten micrograms of solubilized HepG2 cells (hepatocyte cell line), human brain, or purified platelet lysates were analyzed by SDS-PAGE,[17] and immunoblot analysis were completed by using 1:1000 dilutions of either antineurogranin (18% SDS-PAGE) or anticlusterin (8% SDS-PAGE) antibodies. The anticlusterin antibody recognized 2 platelet immunoreactive species under shorter exposure. Although the relative neurogranin and clusterin protein abundances are suboptimally quantified by these analyses, platelet clusterin appears to demonstrate considerable expression when compared with that previously identified in hepatocytes.[31]

Given the importance of complement activation in platelet destruction, the prominent expression of cell-surface clusterin might suggest a role for this protein in normal and pathologic events regulating platelet survival. Interestingly, a clusterin-deficient knockout mouse has been generated that demonstrates enhanced cardiac dysfunction in a model of autoimmune myocarditis.[31] Although these mice apparently have normal baseline hemograms (B. Aronow, personal communication, October 2002), it remains unestablished if they would be predisposed to immune-type thrombocytopenia in systemic models of autoimmunity.

Similarly, the gene encoding an intracellular effector protein that may have key roles in downstream platelet activation events has now been demonstrated to have abundant transcript expression in human platelets. Neurogranin is a highly expressed platelet transcript with its gene product demonstrating a primarily intracellular pattern of distribution. Neurogranin is generally described as a brain-specific, Ca^{2+}-sensitive calmodulin-binding phosphoprotein that is preferentially expressed in neuronal cell bodies and dendrites.[32,33] It is a specific protein kinase C (PKC) substrate that can also be modified by nitric oxide and other oxidants to form intramolecular disulfide bonds. Both its phosphorylation and oxidation state attenuate its binding affinity for calmodulin.[33] In stimulated platelets, PKC generation is linked to various activation pathways such as calcium-regulated kinases, mitogen-activated protein (MAP) kinases, and receptor tyrosine kinases.[1] Thus, these observations suggest that platelet neurogranin may function as a previously unidentified component of a PKC-dependent activation pathway coupled to one (or more) of these effector proteins.

Discussion

These data provide documentation for a unique platelet mRNA profile that may provide a tool for analyzing platelet molecular networks. Nonetheless, the molecular analysis of the platelet transcriptome may be confounded by the constant decay of mRNAs in the absence of new gene transcription, a situation that may, for example, limit the identification of low-abundance transcripts. Similarly, because the circulating platelet pool contains a mixed population of variably aged platelets, a "static" mRNA profile represents an average of this heterogeneous blood pool. Despite these potential limitations, the combination of genomic and proteomic technologies are likely to provide powerful tools for the global analysis of platelet function. Current strategies for cataloging "whole cellular proteomes" are generally accomplished by using 2 developing methodologies: (1) high resolution 2-dimensional polyacrylamide gel electrophoresis (2-DE) with mass spectrometric sequence identification,[34] and (2) microcapillary liquid chromatography with tandem mass spectrometry (μLC-MC/MC).[35] Further modifications of both procedures have been devised for direct comparative studies between 2 cellular proteomes. The introduction of 2-DE differential gel electrophoresis has now made it possible to detect and quantify differences between experimental sample pairs resolved on the same 2-dimensional gel.[36] Likewise, the application of isotope-coded affinity tags to μLC-MC/MC represent a novel means of quantitative analyses between cellular proteomes.[37] The success of both approaches relies on the availability of comprehensive genomic databases and mathematical algorithms for optimal protein identification. Indeed, mathematical modeling studies have demonstrated the need to delineate both protein and mRNA expression levels for optimal definition of intracellular networks.[38] Our data present an initial framework for delineating platelet function by defining the molecular anatomy of human platelets, information that is likely to provide important clues into the dynamic protein interactions regulating normal and pathologic platelet functions. Furthermore, because the platelet transcriptome mirrors the mRNAs derived from precursor megakaryocytes, these analyses may provide insights into the biochemical and molecular events regulating megakaryocytopoiesis and/or proplatelet formation.

References

1 Steinberg P, Hill R. Platelets and megakaryocytes. In: Le R, et al, eds. Wintrobe's Clinical Hematology. Baltimore, MD: Williams & Wilkins; 1999

2 Newman P, Gorski J, White G, Gidwitz S, Cretney C, Aster R. Enzymatic amplification of platelet-specific messenger RNA using the polymerase chain reaction. J Clin Invest. 1988;82:739-743.

3 Kieffer N, Guichard J, Farcet J, Vainchenker W, Breton-Gorius J. Biosynthesis of major platelet proteins in human blood platelets. Eur J Biochem 1987;164:189-195.

4 Weyrich A, Dixon D, Pabla R, et al. Signal-dependent translation of a regulatory protein, Bcl-2, in activated human platelets. Proc Natl Acad Sci USA 1998;95:5556-5561.

5 Benecke BJ, Ben Ze'ev A, Penman S. The control of mRNA production, translation and turnover in

suspended and reattached anchorage-dependent fibroblasts. Cell. 1978;14:931-939.

6. Pabla R, Weyrich AS, Dixon DA, et al. Integrin-dependent control of translation: engagement of integrin alphaIIbbeta3 regulates synthesis of proteins in activated human platelets. J Cell Biol. 1999;144:175-184.

7. Chicurel ME, Singer RH, Meyer CJ, Ingber DE. Integrin binding and mechanical tension induce movement of mRNA and ribosomes to focal adhesions. Nature. 1998;392:730-733.

8. Lindemann S, Tolley N, Eyre J, Kraiss L, Mahoney T, Weyrich A. Integrins regulate the intracellular distribution of eukaryotic initiation factor 4E in platelets. J Biol Chem. 2001;276:33947-33951.

9. Brown EJ, Schreiber SL. A signaling pathway to translational control. Cell. 1996;86:517-520.

10. Rinder H, Schuster J, Rinder C, Wang C, Schwseidler H, Smith B. Correlation of thrombosis with increased platelet turnover in thrombocytosis. Blood. 1998;91:1288-1294.

11. Richards E, Baglin T. Quantitation of reticulated platelets: methodology and clinical application. Br J Haematol. 1995;91:445-451.

12. Robinson M, Mackie I, Khair K, et al. Flow cytometric analysis of reticulated platelets: evidence for a large proportion of non-specific labelling of dense granules by fluorescent dyes. Br J Hematol. 1998;100:351-357.

13. Velculescu V, Zhang L, Vogelstein B, Kinzler K. Serial analysis of gene expression. Science. 1995;270:484-487.

14. Zhang L, Zhou W, Velculescu V, et al. Gene expression profiles in normal and cancer cells. Science. 1997;276:1268-1272.

15. Morin PJ, Sparks AB, Korinek V, et al. Activation of beta-catenin-Tcf signaling in colon cancer by mutations in beta-catenin or APC. Science. 1997; 275:1787-1790.

16. Bahou W, Campbell A, Wicha M. cDNA cloning and molecular characterization of MSE55: a novel human serum constituent protein that displays bone marrow stromal endothelial cell-specific expression. J Biol Chem. 1992;267:13986-13992.

17. Bahou W, Coller B, Potter C, Norton K, Kutok J, Goligorsky M. The thrombin receptor extracellular domain contains sites crucial for peptide ligand-induced activation. J Clin Invest. 1993;91:1405-1413.

18. Heid C, Stevens J, Livak K, Williams P. Real-time quantitative PCR. Genome Res. 1996;6:986-994.

19. Dunn J, McCorkle S, Praissman L; et al. Genome signature tags (GSTs): a system for profiling genomic DNA. Nucleic Acid Res. 2001;29:137-140.

20. Kroll T, Wolfl S. Ranking: a closer look on globalization methods for normalization of gene expression arrays. Nucleic Acids Res. 2002;30:e50.

21. Pruitt KD, Maglott DR. RefSeq and LocusLink: NCBI gene-centered resources. Nucleic Acids Res. 2001;29:137-140.

22. Fox JE, Boyles JK, Reynolds CC, Phillips DR. Actin filament content and organization in unstimulated platelets. J Cell Biol. 1984;98:1985-1991.

23. Safer D, Elzinga M, Nachmias VT. Thymosin beta 4 and Fx, an actin-sequestering peptide, are indistinguishable. J Biol Chem. 1991;266:4029-4032.

24. Wallace DC. Mouse models for mitochondrial disease. Am J Med Genet. 2001;106:71-93.

25. Welle S, Bhatt K, Thornton C. Inventory of high-abundance mRNAs in skeletal muscle of normal men. Genome Res. 1999;9:506-513.

26. Karpatkin S, Charmatz A, Langer RM. Glycogenesis and glyconeogenesis in human platelets. Incorporation of glucose, pyruvate, and citrate into platelet glycogen; glycogen synthetase and fructose-1,6-diphosphatase activity. J Clin Invest. 1970;49:140-149.

27. Raha S, Robinson BH. Mitochondria, oxygen free radicals, and apoptosis. Am J Med Genet. 2001; 106:62-70.

28. Yu J, Zhang L, Hwang P, Rago C, Kinzler K, Vogelstein B. Identification and classification of p53-regulated genes. Proc Nat Acad Sci U S A. 1999; 96:14517-14522.

29. Wang E, Miller L, Ohnmacht G, Liu E, Marincola F. High-fidelity mRNA amplification for gene profiling. Nat Biotechnol. 2000;18:157-459.

30. Kirszbaum L, Sharpe JA, Murphy B, et al. Molecular cloning and characterization of the novel human complement-associated protein, SP-40,40: a link between the complement and reproductive systems. EMBO J. 1989;8:711-718.

31. McLaughlin L, Zhu G, Mistry M, et al. Apolipoprotein J/clusterin limits the severity of murine autoimmune myocarditis. J Clin Invest. 2000;6:1105-1113.

32. Martinez DA, Perez JL, Bernal J, Coloma A. Structure, organization, and chromosomal mapping of the human neurogranin gene (NRGN). Genomics. 1997;41:243-249.

33. Wu J, Li J, Huang K, Huang F. Attenuation of PKC and PKA signal transduction in the neurogranin knockout mouse. J Biol Chem. 2002;277:19498-19505.

34. Gygi S, Rochon Y, Franza B, Aebersold R. Correlation between protein and mRNA abundance in yeast. Mol Cell Biol. 1999;19:1720-1730.

35. Link A, Eng J, Schieltz DM, et al. Direct analysis of protein complexes using mass spectrometry. Nat Biotechnol. 1999;17:676-682.

36. Unlü M, Morgan M, Minden J. Difference gel electrophoresis: a single gel method for detecting changes in protein extracts. Electrophoresis. 1997;18:2071-2077.

37. Gygi S, Rist B, Gerber SA, Turecek F, Gelb MH, Aebersold R. Quantitative analysis of complex protein mixtures using isotope-coded affinity tags. Nat Biotechnol. 1999;17:994-999.

38. Hatizmanikatis V, Lee K. Dynamical analysis of gene networks requires both mRNA and protein expression information. Metabol Eng. 1999;1: 275-281.

Acta Biochimica
Polonica - free

Expression level of Ubc9 protein in rat tissues.

Golebiowski F, Szulc A, Sakowicz M, Szutowicz A, Pawelczyk T.

Department of Molecular Medicine, Medical University of Gdansk, 80-211 Gdansk, Poland.

Ubc9 is a homologue of the E2 ubiquitin conjugating enzyme and participates in the covalent linking of SUMO-1 molecule to the target protein. In this report we describe a simple and efficient method for obtaining pure human recombinant Ubc9 protein. The purified Ubc9 retained its native structure and was fully active in an in vitro sumoylation assay with the promyelocytic leukaemia (PML) peptide as a substrate. In order to better understand the physiology of Ubc9 protein we examined its levels in several rat tissues. Immunoblot analyses performed on tissue extracts revealed quantitative and qualitative differences in the expression pattern of Ubc9. The Ubc9 protein was present at a high level in spleen and lung. Moderate level of Ubc9 was detected in kidney and liver. Low amount of Ubc9 was observed in brain, whereas the 18 kDa band of Ubc9 was barely visible or absent in heart and skeletal muscle. In heart and muscle extracts the Ubc9 antibodies recognized a 38 kDa protein band. This band was not visible in extracts of other rat tissues. A comparison of the relative levels of Ubc9 mRNA and protein indicated that the overall expression level of Ubc9 was the highest in spleen and lung. In spleen, lung, kidney, brain, liver and heart there was a good correlation between the 18 kDa protein and Ubc9 mRNA levels. In skeletal muscle the Ubc9 mRNA level was unproportionally high comparing to the level of the 18 kDa protein. The presented data indicate that in the rat the expression of the Ubc9 protein appears to have some degree of tissue specificity.

Protein abundancy and mRNA levels of the adipocyte-type fatty acid binding protein correlate in non-invasive and invasive bladder transitional cell carcinomas.

Gromova I, Gromov P, Wolf H, Celis JE.

Department of Medical Biochemistry and Danish Centre for Human Genome Research, The University of Aarhus, Aarhus C, Denmark.
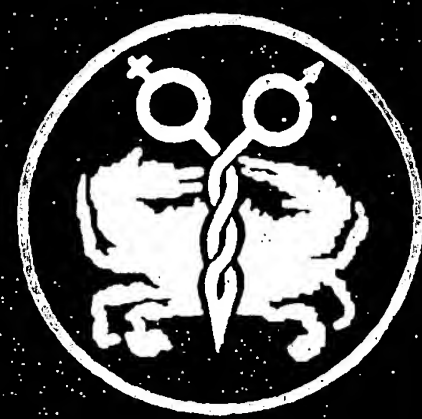
The adipocyte type fatty acid-binding protein (A-FABP) is a small molecular weight fatty acid-binding protein whose expression correlates both with the grade of atypia and the stage of bladder transitional cell carcinomas (TCCs). To determine if the protein abundancy correlates with the mRNA levels in non-invasive and invasive lesions, we have analysed fresh TCCs (grade II, Ta; grade III, T2-4) by two-dimensional polyacrylamide gel electrophoresis (2D-PAGE) and measured the mRNA levels using the reverse transcription linked polymerase chain reaction (RT-PCR). Overall, the results showed a good correlation between protein abundancy and mRNA levels, indicating that the lack of expression of the protein observed in some lesions reflects low levels of transcription of the A-FABP gene rather than translational regulation. In addition, our studies showed that the loss of A-FABP protein observed in some tumors is not compensated by an increase in the skin fatty acid-binding protein PA-FABP, as is the case in the A-FABP knockout mice.

International Journal of Oncology

An international journal devoted to Oncology Research and Cancer Treatment

Protein abundancy and mRNA levels of the adipocyte-type fatty acid binding protein correlate in non-invasive and invasive bladder transitional cell carcinomas

IRINA GROMOVA[1], PAVEL GROMOV[1], HANS WOLF[2] and JULIO E. CELIS[1]

[1]Department of Medical Biochemistry and Danish Centre for Human Genome Research, The University of Aarhus, DK-8000, Aarhus C; [2]Department of Urology, Skejby Hospital, Aarhus, Denmark

Abstract. The adipocyte type fatty acid-binding protein (A-FABP) is a small molecular weight fatty acid-binding protein whose expression correlates both with the grade of atypia and the stage of bladder transitional cell carcinomas (TCCs). To determine if the protein abundancy correlates with the mRNA levels in non-invasive and invasive lesions, we have analysed fresh TCCs (grade II, Ta; grade III, T_{2-4}) by two-dimensional polyacrylamide gel electrophoresis (2D-PAGE) and measured the mRNA levels using the reverse transcription linked polymerase chain reaction (RT-PCR). Overall, the results showed a good correlation between protein abundancy and mRNA levels, indicating that the lack of expression of the protein observed in some lesions reflects low levels of transcription of the A-FABP gene rather than translational regulation. In addition, our studies showed that the loss of A-FABP protein observed in some tumors is not compensated by an increase in the skin fatty acid-binding protein PA-FABP, as is the case in the A-FABP knockout mice.

Introduction

Bladder cancer accounts for 4.7% of all human cancers diagnosed. The spectrum of bladder tumors is broad with various histological types that include transitional cell carcinomas (TCCs), squamous cell carcinomas (SCCs), and adenocarcinomas (1-3). TCCs are by far the most prevalent tumors as they represent nearly 95% of all bladder cancers in the Western Hemisphere. At first presentation, about 70% of the urinary bladder TCCs are diagnosed as differentiated superficial lesions that are confined either to the mucosa (Ta), or to the underlying connective tissue (T_i). The rest correspond to highly invasive, poorly differentiated tumors.

Non-invasive TCCs occur as two distinct growth patterns, papillary and non-papillary (flat) lesions (1,2), that display significant differences in their malignant potential and that are believed to originate from different genetic alterations (4-6). Papillary carcinomas usually correspond to low-grade lesions which frequently recur multiple times. These tumors begin as areas of hyperplasia that later undergo a process of dedifferentiation (grades I-IV). Invasive tumors may arise from these lesions, but often are derived from non-papillary carcinoma in situ that usually is of high grade at presentation and tend to invade and progress to muscle invasion and metastatic disease.

To date, many attempts have been made to pinpoint genetic changes that underly progression of bladder cancer as well as to identify molecular markers that correlate with tumor progression. Cytogenetic studies and molecular genetic data have shown that chromosomes 3p, 4p, 4q, 5q, 8p, 9p, 9q, 11p, 13q, 14q, 17p and 18q are frequently altered in bladder urothelial tumors (4,5 and refs. therein), and as a whole they have supported the notion that bladder cancer is a multistep process. Recently, Spruck et al (6) showed that chromosome 9 alterations occur early during development, while p53 mutations appear later in the process and confer invasive properties. The situation however is reverse in the case of Cis, as a large fraction of these lesions contain p53 mutations (5,6,8,9). Besides pointing towards two divergent pathways of bladder tumor progression, these studies implied that the order in which the genetic changes occur is important in determining the outcome of the lesion.

Assessment of bladder cancer is based on a thorough pathological examination of biopsy material which establishes the histological type of the tumor, its degree of differentiation (grade), and depth of invasion of the bladder wall (staging) (10-12). In spite of strict criteria for the pathological assessment of these lesions, there exist a significant inter-pathologist variation, a fact that emphasises the need for objective markers that may aid their classification. With this in mind, we are exploring the possibility of using proteome (13)

---

expression profiles of these lesions as fingerprints to define their grade of atypia and eventually their stage (3,14). So far, more than 400 tumors of various grades and stages have been analysed by two-dimensional polyacrylamide gel electrophoresis (2D PAGE), and preliminary experiments have shown that even though the overall protein expression profiles of tumors of the same grade and stage are very similar, there are important differences suggesting that morphologically 'identical' TCCs may be further subdivided (1). Of the biomarkers of TCC progression identified so far, the adipocyte-type fatty acid binding protein (A-FABP) is perhaps one of the most interesting as the levels of this polypeptide have been shown to correlate both with the grade of atypia as well as with the stage of the disease (3). Given the putative importance of A-FABP as a progression marker, and since Anderson and Seilheimer (15) recently showed that post-transcriptional regulation of gene expression is a frequent phenomena in higher organisms, we have compared the levels of A-FABP mRNA and protein in non-invasive and invasive bladder TCCs expressing and lacking this protein.

Materials and methods

Tumors. Fresh bladder tumors were obtained immediately after transurethral resection. The grade and clinical stage of the tumors were determined by the pathologist at the Aarhus Municipal hospital. Clean tumors devoid of blood clots were divided into small pieces for 2D PAGE and DNA, and RNA preparation. The latter were immediately frozen in liquid nitrogen and store at -80°C until use.

[35S]-methionine labeling and 2D-PAGE. In a few cases, small tumor pieces were labeled with [35S]-methionine as previously described (3). 2D-PAGE was performed according to published procedures (16; see also http://biobase.dk/cgi-bin/celis).

RT-PCR. Frozen tumor samples were ground to powder in liquid nitrogen and total RNA was isolated using the acid guanidium isothiocyanate/phenol chloroform extraction procedure (17). The samples were treated with RNase-free DNases I (Pharmacia) to eliminate contaminating genomic DNA using the protocols recommended by the supplier. Poly(A)⁺ RNA was prepared using Poly (A) Quick columns according to the manufacturer's instructions (Stratagene). The synthesis of cDNA for RT-PCR reactions were carried out using the Gibco BRL SuperScript Kit. Two µg of total RNAs was mixed with oligo -dT11 primer. PCR buffer, MgCl$_2$ (25 mM), 0.1 M DDT and 10 mM dNTP. The mixture was incubated at 42°C for 5 min followed by the addition of SuperScript II reverse transcriptase and further incubation at 42°C for 50 min. The reaction was terminated by raising the temperature to 70°C for 15 min, followed by additional incubation at 37°C for 20 min in the presence of RNase H to deplete the RNA. Primers for known and cloned genes were purchase from Pharmacia as follows: A-FABP, Upper (from 186-208 bp) 5'-GATCATCAGTGTGAATGGGGAT-3'/ lower (from 374-397 bp) 5'-CATCCTCTCGTTTTCTCTTT ATG-3'; β-actin upper 5'-GAGGTTGGCTCTGACTGTACC AC-3'/lower 5'-CTCATTCAGCTCTCGGAACATCTCG-3'.

Table I. Expression of A-FABP in non-invasive and invasive bladder TCCs:

TCC	Grade/stage	Level of A-FABP protein[a]	Level of A-FABP mRNA[b]
154	GrII/Ta	+	++
166-5	GrII/Ta	-	+
532-1	GrII/Ta	++++	++++
533-1	GrII/Ta	+	+
607-1	GrII/Ta	-	-
692-1	GrII/Ta	+++	+++
709-1	GrII/Ta	-	-
763-1	GrII/Ta	++	++
581-1	GrII/Ta	+	+
616-1	GrII/Ta	+	++
428-5	GrIII/T$_2$-T$_3$	-	-
570-2	GrIII/T$_2$-T$_3$	-	-
612-3	GrIII/T$_2$-T$_3$	-	-
711-1	GrIII/T$_2$-T$_4$	-	-
712-1	GrIII/T$_2$-T$_4$	-	-
727-1	GrIII/T$_2$-T$_4$	-	-

[a]The levels of a A-FABP protein were determined based on the visual analysis of Coomassie Brilliant Blue stained gels and represent the average estimate of at least two different runs. Tumors scored as positive differed significantly with respect to the levels of the protein, and therefore are indicated with either four (very high), three (high), two (medium) and one (low) cross (see also Fig. 1); [b]The mRNA levels were determined based on the intensity of Ethidium Bromide stained cDNA bands separated on agarose gel using the Bio-Rad Gel Doc 1000 system and represent the average estimate of at least three independent experiments. Corresponding mRNA levels are represented by crosses as described above.

PCR reactions were performed in a Progene thermal cycler using the Advantage Klen Tag Polimerase (Clontech). The cycling parameters consisted of 30 sec of denaturation at 94°C, with annealing of 30 sec at 60°C for B-actin or at 64°C for A-FABP. The extension time was for 2 min at 68°C for 29-40 cycles with the final extension of 7 min at 68°C. The PCR products were separated on 1.5% agarose gel electrophoresis followed by ethidium bromide staining and photography under UV light.

Results

A-FABP protein levels in non-invasive and invasive TCCs. One hundred suspected TCCs removed at the Department of Urology, Skejby Hospital, were analysed by high resolution 2D PAGE and Coomassie Brilliant Blue staining. Of these, 10 grade II, Ta TCCs (Table I) were chosen to correlate A-FABP protein and mRNA levels as these lesions yielded acceptable protein profiles both in terms of their purity as
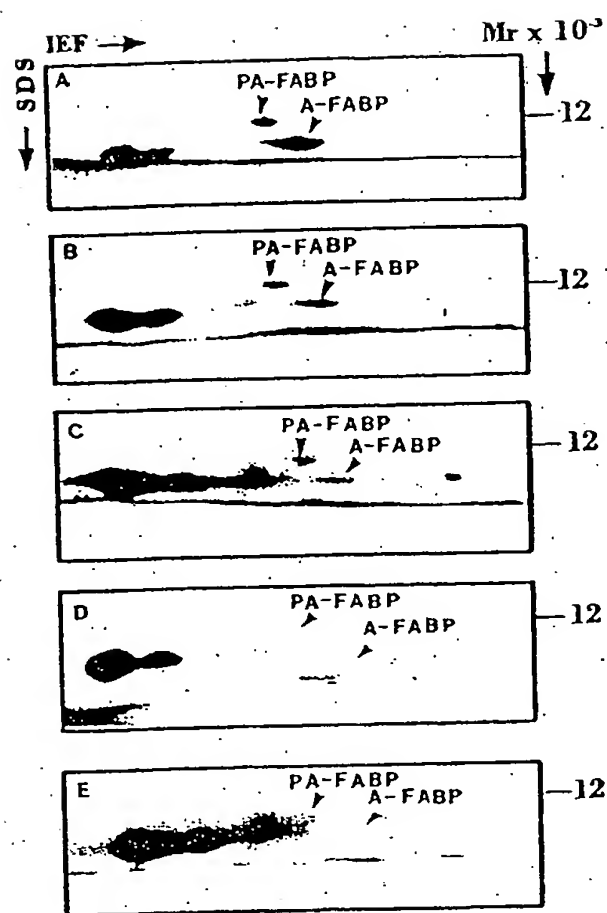
Figure 1. IEF 2D gels of whole cellular extracts from non-invasive and invasive TCCs. A. TCC 532-1; B. TCC-692-1; C. TCC 763- 1; D. TCC 709-1 and E. TCC 711-1. Only the relevant area of the gels are shown.

Figure 2. RT-PCR analysis of A-FABP mRNA expression in non-invasive (GrII, Ta) and invasive TCCs (Gr III, T_2-T_4). For RT-PCR analysis, the ss c-DNA was synthesized by Reverse Transcriptase using total RNA, and used for RT-PCR amplification. The PCR products were resolved on 1.5% agarose gels and visualised under UV light following ethidium bromide staining. The A-FABP panels show the results of amplifications where the pair of gene specific primers was used to generate the 220 bp DNA fragment. Amplification of A-FABP was obtained after 30 cycles of PCR. The ß-actin panels represent the amplification of the ß-actin gene, which was used as an internal control to confirm that equal amounts of c-DNA were used in each reaction.

assessed by monitoring for the absence of vimentin (contamination with connective tissue) and desmin (contamination with smooth muscle cells), as well as polypeptide resolution. In addition, reasonable amounts of these tumors were available for mRNA preparation.

Table I shows the levels of A-FABP protein expression in the 10 tumors analysed by 2D PAGE. The data were scored entirely based on the visual analysis of Coomassie Brilliant Blue stained gels and represent an average estimate of at least two different runs. Tumors scored as positive differed significantly with respect to the levels of this protein, and therefore are indicated with either four (very high), three (high), two (medium) and one cross (low). Representative examples of Coomassie stained 2D gels of tumors exhibiting very high (TCC 532-1, Fig. 1A), high (TCC 692-1; Fig. 1B), medium (TCC 763-1, Fig. 1C) and undetectable levels (TCC 709-1 and TCC 711-1 Fig. 1D-E) of A-FABP are shown in Fig. 1 (only the relevant area of the gels are shown).

A-FABP mRNA levels in non-invasive grade II, Ta TCCs.
Since in many instances only a limited amount of fresh tumor was available, we used RT-PCR to determine the levels of A-FABP mRNA in the ten TCCs analysed by 2D PAGE (Fig. 1). Following amplification, the PCR products were analysed by conventional 1.5% agarose gel electrophoresis and visualised by ethidium bromide staining as shown in Fig. 2. The amount
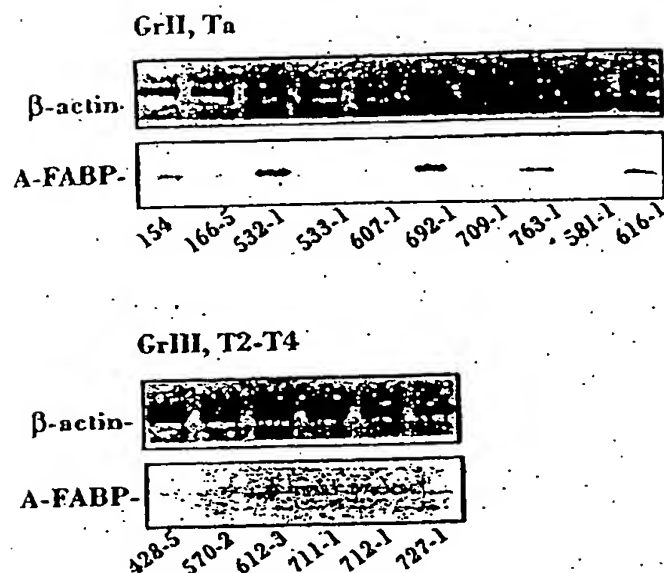
of cDNA in each lane was normalised using several house-keeping genes so as to achieve a more accurate assessment of the expression of the A-FABP mRNA. As shown in Fig. 2, TCC 532-1 exhibited the highest amount of A-FABP mRNA, followed by TCCs 692-1, 763-1, 616-1, 581-1, 154-1, 166-5 and 533-1. Undetectable levels of A-FABP mRNA were observed in the case of TCCs 607-1 and 709-1 (Fig. 2). Relative mRNA levels for the ten TCCs are given in Table I.

A-FABP protein and mRNA levels in invasive grade III, T_{2-4} TCCs. Of the invasive TCCs (grade III, T_{2-4}) analysed by 2D PAGE only six yielded reasonable protein profiles for further study. As shown in Table I, none of these lesions expressed detectable levels of A-FABP as determined by Coomassie Brilliant Blue staining (Fig. 1E, TCC 711-1). In line with these results, the RT-PCR analysis of these tumors also revealed undetectable level of A-FABP mRNA (Fig. 2, Gr III T_2-T_4; Table I).

Loss of A-FABP protein is not compensated by an increase in PA-FABP. Recent studies of A-FABP knockout mice have shown that the loss of A-FABP in fat tissue is compensated by an increase in the skin fatty acid-binding protein mal1 (18). Our studies, however, indicated that the human homologue of mal1, PA-FABP (19), did not compensate for the loss of A-FABP either in the non-invasive or the invasive tumors analysed in this study (Fig. 1D and E). In addition, Fig. 3 shows 2D gels of [^{35}S]-methionine labeled proteins from two grade II, Ta TCCs (192-4, T_a; Fig. 3A and 192-4, T_a; Fig. 3B).
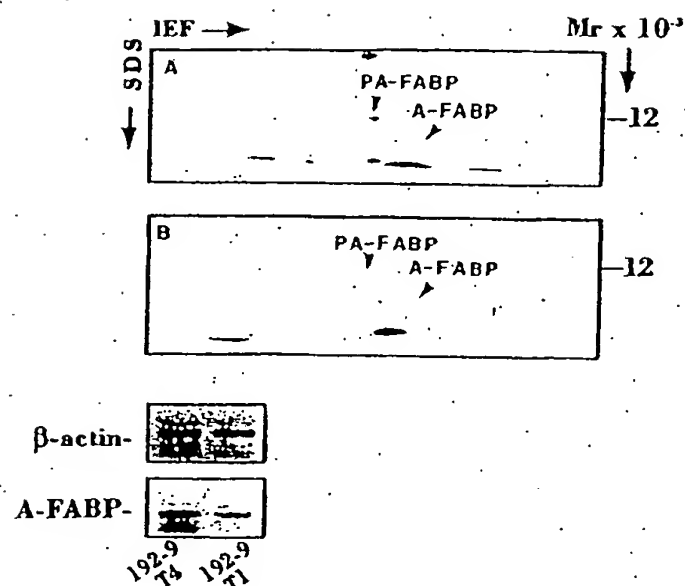
Figure 3. Levels of A-FABP and PA-FABP protein in grade II, Ta tumors resected from the same patient. The two upper panels show the 2D gel autoradiograms of [³⁵S]-methionine labeled proteins from TCCs (grade II, Ta) resected from the same patient. A, TCC 192-9 tumor 4 and B,- TCC 192-9 tumor 1. Only the relevant area of the autoradiograms are shown. The low panel shows the RT-PCR analysis of A-FABP mRNA expression in the same tumors (see also legend to Fig. 2).

which differ significantly in their levels of A-FABP protein and mRNA (Fig. 3, low panel). As shown in Fig. 3, the decrease in A-FABP observed in TCC 129-4, T_1 is not accompanied by an increase in the PA-FABP protein (Fig. 1E).

Discussion

Of the TCC progression markers identified to date, A-FABP is perhaps one of the most interesting as its presence correlates both with the grade of atypia (p=0.0006) and the stage of the disease (p=0.0269) (3). A-FABP is a low molecular weight protein belonging to a cytosolic multigene family of lipid-binding proteins that include heart, liver, intestinal, muscle, brain, skin and epithelial isoforms (20). Members of the FABP family are highly expressed in differentiated cells and show narrow tissue distribution. Their precise function is at present unknown, although there is evidence suggesting that they may play roles in intracellular lipid transport and metabolism, signal transduction (21,22) as well as growth control and differentiation (23). The role in signal transduction has been inferred from the fact that long-chain fatty acids and their metabolites can act as primary and second messengers in specific signalling pathways (24). Recently, it has been shown that A-FABP may play a central role in the pathway that links obesity with insulin resistance, most likely by connecting the fatty acid metabolism with the expression of TNF-α (18). Furthermore, there is evidence indicating that the A-FABP gene contains sequence information necessary for differentiation-dependent expression in adipocytes (25). Our own data derived from the study of TCCs and normal urothelium suggest that A-FABP may be required for normal urothelium differentiation (1), as may be the case for PA-FABP in the skin (19).

Considering the potential prognostic value of A-FABP protein and/or mRNA in TCC progression it was important to determine if the levels of both type of macromolecules correlated both in the non-invasive and the invasive lesions expressing and lacking A-FABP. The need for such correlation was underlined by recent studies of Anderson and Seilhamer (15), who reported a lack of overall correlation between the mRNA and protein levels of 45 rat proteins analysed by 2D PAGE in combination with cDNA arrays. Their data yielded a correlation coefficient of 0.45 which is half way between weak and perfect correlation. Clearly, our data showed a very good correlation between the protein and mRNA levels of A-FABP in all tumors analysed indicating that the loss of A-FABP protein observed in some tumors is not due to post-transcriptional regulation.

Recently, knockout mice carrying a null mutation in the aP2 gene encoding for A-FABP was produced (18). These animals do not show an obvious morphological or metabolic phenotype, but exhibit a 20-fold increase in the levels of the keratinocyte type FABP (mal1), which may compensate for the loss of the deleted gene (18). The human homologue of the mal1 gene, PA-FABP, was cloned in our laboratory and has been shown to be highly upregulated in psoriatic skin as well as in abnormally differentiated primary keratinocytes (19). PA-FABP is expressed in normal urothelium together with A-FABP (3), and ongoing studies in the laboratory have shown that its level decreases significantly as tumors progress. Interestingly, the studies reported in this article did not revealed a compensatory up- or down-regulation of PA-FABP in the TCCs analysed, supporting the contention that PA-FABP may also play a role in cell growth and differentiation (19).

References

1. Friedell GH, Nagy GK and Cohen SM: The pathology of human bladder cancer and related lesions. In: The Pathology of Bladder Cancer. I. Bryan GT and Cohen SM (eds). CRC Press Inc., Roca Baton FL, pp11-42, 1983.
2. Pauli BU, Alroy J and Weinstein RS: The ultrastructure and pathology of urinary bladder cancer. In: The Pathology of Bladder Cancer. II. Bryan GT and Cohen SM (eds). CRC Press Inc., Roca Baton FL, pp41-140, 1983.
3. Celis JE, Ostergaard M, Basse B, Celis A, Lauridsen JB, Ratz GP, Andersen I, Hein B, Wolf H, Ørntoft TF and Rasmussen HH: Loss of adipocyte-type fatty acid binding protein and other protein biomarkers is associated with progression of human bladder transitional cell carcinomas. Cancer Res 56: 4782-4790, 1996.
4. Heney NM, Ahmed S, Flanagan MJ, Frable W, Corder MP, Hafermann MD and Hawkins IR: Superficial bladder cancer: progression and recurrence. J Urol 130: 1083-1086, 1983.
5. Simoneau AR and Jones PA: Bladder cancer: the molecular progression to invasive disease (Review). World J Urol 12: 89-95, 1994.
6. Spruck CH, Ohneseit PF, Gonzalez-Zulueta M, Esrig D, Miyao N, Tsaim YC, Lerner SP, Schmutte C, Yang AS and Cote R: Two molecular pathways to transitional cell carcinoma of the bladder. Cancer Res 54: 784-788, 1994.

7. Rosin MP, Cairns P, Epstein JI, Schoenberg MP and Sidransky D: Partial allelotype of carcinoma *in situ* of the human bladder. Cancer Res 55: 5213-5216, 1995.

8. Birchmeier W and Birchmeier C: Epithelial-mesenchymal transitions in development and tumour progression. In: Epithelial-Mesenchymal Interactions in Cancer. Goldberg ID and Rosen EM (eds). Birkhäuser, Basel, pp1-15, 1995.

9. Sidransky D, von Eschenbach A, Tsai YC, Jones P, Summerhayes I, Marshall F, Paul M, Green P, Hamilton SR, Frost P, et al: Identification of p53 gene mutations in bladder cancers and urine samples. Science 252: 706-709, 1991.

10. Lopez-Beltran A, Croghan GA, Croghan I, Huben RP, Mettlin C and Gaeta JF: Prognostic factors in survival of bladder cancer. Cancer 70: 799-807, 1992.

11. Kern WH: The grade and pathologic stage of bladder cancer. Cancer 53: 1185-1189, 1984.

12. Jordan AM, Weingarten J and Murphy WM: Transitional cell neoplasms of the urinary bladder. Can biologic potential be predicted from histologic grading? Cancer 60: 2766-2774, 1987.

13. Wilkins MR, Sanchez JC, Gooley AA, Appel RD, Humphery-Smith I, Hochstrasser DF and Williams KL: Progress with proteome projects: why all proteins expressed by a genome should be identified and how to do it. Biotechnol Genet Eng Rev 13: 19-50, 1996.

14. Ostergaard M, Rasmussen HH, Nielsen HV, Vorum H, Ørntoft TF, Wolf H and Celis JE: Proteome profiling of bladder squamous cell carcinomas: identification of markers that define their degree of differentiation. Cancer Res 57: 4111-4117, 1997.

15. Anderson L and Seilhamer J: A comparison of selected mRNA and protein abundances in human liver. Electrophoresis 18: 533-537, 1997.

16. Celis JE, Ratz G, Basse B, Lauridsen JB and Celis A: High resolution two-dimentional gel electrophoresis of proteins: isoelectric focusing and non-equilibrium pH gradient electrophoresis (NEPHGE). In: Cell Biology: A Laboratory Handbook. III. Celis JE (ed). Academic Press, pp222-230, 1994.

17. Chomczynski P and Sacchi N: Single-step method of RNA isolation by acid guanidinium thiocyanate-phenol-chloroform extraction. Anal Biochem 162: 156-159, 1987.

18. Hotamisligil GS, Johnson RS, Distel RJ, Ellis R, Papaioannou VE and Spiegelman BM: Uncoupling of obesity from insulin resistance through a targeted mutation in aP2, the adipocyte fatty acid binding protein. Science 274: 1377-1379, 1996.

19. Madsen P, Rasmussen HH, Leffers H, Honore B and Celis JE: Molecular cloning and expression of a novel keratinocyte protein psoriasis-associated fatty acid-binding protein (PA-FABP) that is highly up-regulated in psoriatic skin and that shares similarity to fatty acid-binding proteins. J Invest Dermatol 99: 299-305, 1992.

20. Veerkamp JH, Paulussen RJ, Peeters RA, Maatman RG, van Moerkerk HT and van Kuppevelt TH: Detection, tissue distribution and (sub)cellular localization of fatty acid-binding protein types. Mol Cell Biochem 98: 11-18, 1990.

21. Glatz JF, Vork MM, Cistola DP and van der Vusse GJ: Cytoplasmic fatty acid binding protein: significance for intracellular transport of fatty acids and putative role on signal transduction pathways. Prostaglandins Leukot Essent Fatty Acids 48: 33-41, 1993.

22. Spitsberg VL, Matitashvili E and Gorewit RC: Association and coexpression of fatty-acid-binding protein and glycoprotein CD36 in the bovine mammary gland. Eur J Biochem 230: 872-878, 1995.

23. Yang Y, Spitzer E, Kenney N, Zschiesche W, Li M, Kromminga A, Muller T, Spener F, Lezius A, Veerkamp JH, et al: Members of the fatty acid binding protein family are differentiation factors for the mammary gland. J Cell Biol 127: 1097-1109, 1994.

24. Glatz JF, Borchers T, Spener F and van der Vusse GJ: Fatty acids in cell signalling: modulation by lipid binding proteins. Prostaglandins Leukot Essent Fatty Acids 52: 121-127, 1995.

25. Hunt CR, Ro JH, Dobson DE, Min HY and Spiegelman BM: Adipocyte P2 gene: developmental expression and homology of 5'-flanking sequences among fat cell-specific genes. Proc Natl Acad Sci USA 83: 3786-3790, 1986.

Expression of the pS2 gene in breast tissues assessed by pS2-mRNA analysis and pS2-protein radioimmunoassay.

Hahnel E, Robbins P, Harvey J, Sterrett G, Hahnel R.

Department of Pathology, University of Western Australia, Queen Elizabeth II Medical Centre, Nedlands.

The expression of the pS2 gene in breast tissues was assessed by measuring pS2-protein using a radioimmunoassay, and by determining pS2-mRNA using Northern blotting. There was a good correlation between the two measurements, indicating that expression of the pS2 gene in breast tissues may be assessed by either method. Since radioimmunoassay is technically easier and more efficient than Northern blotting, radioimmunoassay will be the method of choice in routine applications.

Breast Cancer Research and Treatment

Marc E. Lippman, MD, editor-in-chief

Kluwer Academic Publishers

Breast Cancer Research and Treatment

Marc E. Lippman, M.D. [1] (Editor-in-Chief), Gary C. Chamness, Ph.D. [2] / Robert L. Dickson, Ph.D. [1] (Editors), C. Kent Osborne, M.D. [2] / Gary M. Clark, Ph.D. [2] (Associate Editors)

[1] Vincent T. Lombardi Cancer Research Center, Georgetown University, Washington DC, USA

[2] University of Texas Health Science Center at San Antonio, San Antonio, TX, USA

Brief communication

Expression of the pS2 gene in breast tissues assessed by pS2-mRNA analysis and pS2-protein radioimmunoassay

Erika Hähnel, Peter Robbins, Jennet Harvey, Gregory Sterrett and Roland Hähnel
Department of Pathology, University of Western Australia, Queen Elizabeth II Medical Centre, Nedlands, 6009, Western Australia

Key words: breast tissue, pS2-mRNA, pS2 protein, radioimmunoassay

Summary

The expression of the pS2 gene in breast tissues was assessed by measuring pS2-protein using a radioimmunoassay, and by determining pS2-mRNA using Northern blotting. There was a good correlation between the two measurements, indicating that expression of the pS2 gene in breast tissues may be assessed by either method. Since radioimmunoassay is technically easier and more efficient than Northern blotting, radioimmunoassay will be the method of choice in routine applications.

Introduction

Expression of the pS2 gene is controlled by estrogen. This was first described in the MCF-7 breast cancer cell line [1]. pS2 expression has since been reported to be useful as a prognostic indicator [2, 3], although this was not confirmed in another series [4].

pS2 expression may be assessed in tissue homogenates by analysis of pS2-mRNA [5], by radioimmunoassay of the pS2-protein [2], or by immunocytochemical detection of the pS2 protein in tissue sections [5]. It was the aim of this study to establish the correlation between pS2-mRNA and pS2-protein by radioimmunoassay in a series of tissues obtained from mastectomy specimens performed for carcinoma of the breast. Primary breast carcinoma tissue, metastatic carcinoma within axillary nodes, and macroscopically benign breast tissue were examined.

Materials and methods

Breast tissues

Tissue specimens from mastectomies performed for carcinoma of the breast were examined. 32 primary breast carcinomas, 10 axillary lymph nodes containing metastatic breast carcinoma, and 20 samples of uninvolved breast tissue were analyzed for pS2 expression.

The primary breast carcinomas were histologically classified using a conventional subclassification. The presence or absence of primary tumour was assessed. The presence of metastatic carcinoma within lymph nodes studied was verified by histological examination of the node remnant after sampling.

'Uninvolved' breast tissue was sampled from sites well removed from the primary breast tumour (usually in another quadrant of the breast), and was selected only if the tissue appeared macroscopically unremarkable. Tissue sampling occurred imme-

Address for offprints: R. Hähnel. University Department of Pathology. The Queen Elizabeth II Medical Centre. Nedlands 6009, Western Australia

diately upon arrival of the mastectomy specimen in the laboratory, with minimal delays between removal and sampling.

Tissues for pS2 analysis were snap frozen in liquid nitrogen and stored at −70°C until processed.

Extraction of RNA and determination of pS2-mRNA

Details of the procedure have been described in our previous paper [6]. Briefly, the deep-frozen tissue was homogenized in a micro-dismembrator. The homogeneous powder was extracted with guanidiniumisothiocyanatephenolchloroformisoamylalcohol, and RNA was precipitated with isopropanol. The washed RNA pellet was dissolved in SDS and glyoxylated, and the RNA preparation loaded onto agarose gel. After electrophoresis the gel was capillary blotted onto Zeta-probe membranes. Membranes were hybridized overnight with cDNA probes pS2 and 36B4, which were labeled with [α^{32}P] dCTP by nick translations. Washed membranes were exposed to Kodak X-omat AR film. Relative intensities of the mRNA bands were assessed visually as not detectable, very weak, weak, medium, strong, and very strong, taking the intensities of the ubiquitous 36B4 bands into account.

Radioimmunoassay of pS2-protein

Deep frozen specimens were pulverized with a microdismembrator. The tissue powder was suspended in 10 volumes of pH 7.5 phosphate buffer. The homogenate was centrifuged in a refrigerated centrifuge at 4°C for 60 minutes at 2600 x g. The supernatant was removed with a Pasteur pipette, carefully avoiding the fat layer on the top. The protein concentration in the supernatant was estimated by use of the Coomassie dye-binding method [7]. An aliquot of the supernatant was diluted to a protein concentration between 1 and 2 mg/ml before assay of the pS2-protein. In one case the protein concentration of the supernatant was well below 1 mg/ml.

The estimation of the pS2-protein was performed using a solid phase, two-site radioimmunoassay. The kits were bought from CIS Biointernational, Gif-sur-Yvette, France (ELSA-PS2). In this method the molecules of pS2 are sandwiched between two monoclonal antibodies; the first one is coated on the ELSA solid phase, the second one is radiolabeled with 125-iodine. The radioactivity bound to the ELSA is proportional to the concentration of pS2-protein. Details of the procedure are supplied with the kit [8].

Results and discussion

32 primary breast carcinomas, metastatic breast carcinoma in 10 lymph nodes, and 20 samples of benign breast tissue from mastectomies were investigated. Two of the carcinomas were of the infiltrating lobular type, two were ductal carcinomas in situ, one was a multicentric invasive ductal carcinoma, all others were invasive ductal carcinomas.

Examples of pS2 Northern blots have been shown in our previous paper [6] which demonstrate that undegraded pS2-mRNA can be isolated by the method used.

The results of the pS2-protein and pS2-mRNA assays are shown on Fig. 1. There was a good correlation between the two types of results. When pS2-mRNA could not be detected by Northern blot, pS2-protein results were usually below 1 ng/mg protein (22 of 30), or between 1 and 3.7 ng/mg (6 of 30). Two were exceptions (7.7 and 14.6); one of them could have been due to the very low protein content in the cytosol which would lead to a large pS2 value and an associated error. There was no explanation for the other high result. Very weak pS2-mRNA signals on Northern blots corresponded to pS2-protein values between 1.1 and 19.2 with an average of 6.6 ng/mg protein (median 5.7). The mean and median pS2-protein concentration in the tissue with weak pS2-mRNA signals were 14.3 and 10.7 ng/mg protein, respectively. The average pS2-protein concentration increased to 32.7 (median 31.5) ng/mg protein for tissues assessed as medium pS2-mRNA intensity, and to 43.3 (median 53.8) ng/mg protein for tissues with strong or very strong

pS2-mRNA signals. These values should be used as an approximate guide only, since the number of samples in the various groups was fairly small. One-way analysis of variance confirmed that the means of the pS2-protein values in the groups made up according to their pS2-mRNA signal intensity, were significantly different ($p < 10^{-6}$).

If the pS2 gene is expressed, its expression is on average greater in breast carcinomas than in uninvolved breast tissue. If one takes pS2-protein values above 4 ng/mg protein as cut-off, the average pS2-protein in 14 breast cancers was 34.3 (median 35.2), while it was only 18.1 (median 13.8) in 12 uninvolved breast tissue samples. If the cut-off is taken at 10 ng/mg protein, average pS2-protein in breast carcinoma is also about twice the level of uninvolved tissue. There were not enough lymph node metastases which expressed the pS2 gene to allow a comparison with carcinoma or uninvolved breast tissue.

Recent preliminary results of pS2 by radioimmunoassay [9] are similar to ours for breast cancer but considerably lower than our results for normal breast tissue.

The values of the pS2-protein measured obviously depend on the protein used for calibration. We used the pS2-protein standards supplied with the CIS kit, which according to the supplier gave values from 0 to 740 ng/mg protein in a series of 205 breast cancer cytosols. Previously, a different standard had been used for presumably the same series of breast carcinomas [2], and a conversion factor to current standards is given as 2.8 [8].

It was noticed that the correlation between pS2-protein and pS2-mRNA was better in breast carcinoma specimens than in uninvolved breast tissue. This is unexplained, though it could be due to the variable content of cell or tissue types in adjoining parts of a specimen, a variation more likely to occur in our sampling of non-malignant breast tissue compared to sampling of carcinomas. A similar variability in breast carcinoma specimens will probably have a smaller influence on the pS2 results, since the malignant cells - if they do express the pS2 gene - contain more pS2-protein than normal breast.

CORRELATION OF pS2 - mRNA AND pS2 - PROTEIN
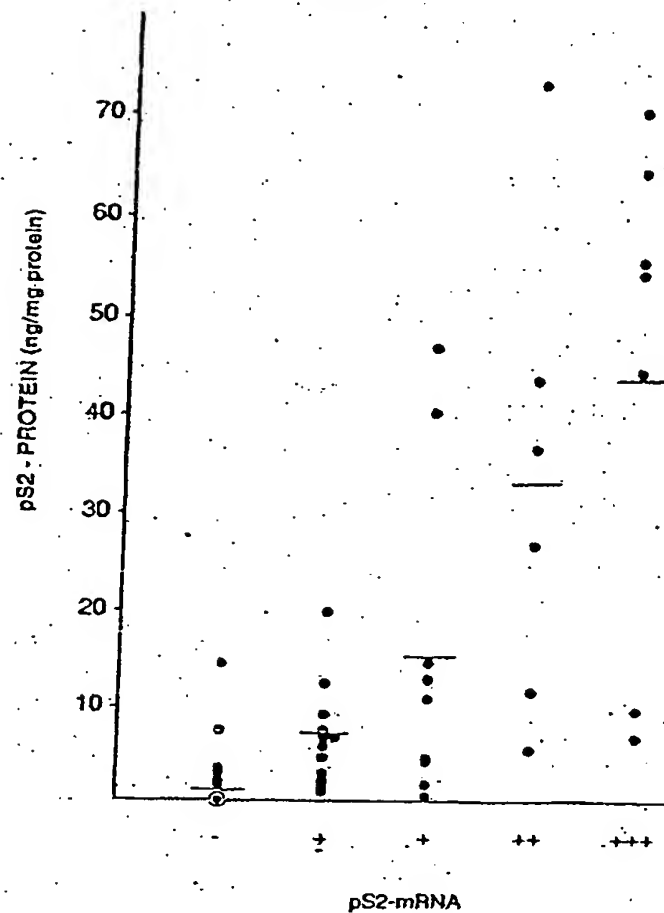

Fig. 1. Correlation between pS2-protein by radioimmunoassay and pS2-mRNA by Northern blot. ⊙ = 22 results below 1. The horizontal lines indicate the mean values.

Acknowledgements

References

1. Masiakowski P, Breathnach R, Bloch J, Gannon F, Krust A, Cham-

bon P: Cloning of cDNA sequences of hormone-regulated genes from the MCF-7 human breast cancer cell lines. Nucleic Acids Res 10: 7895–7903, 1982

2. Foekens JA, Rio MC, Seguin P, Van Putten WLJ, Fauque J, Nap M, Klijn JGM, Chambon P: Predication of relapse and survival in breast cancer patients by pS2 protein status. Cancer Res 50: 3832–3837, 1990

3. Foekens JA, Van Putten WLJ, Portengen H, Rodenburg CJ, Reubi JC, Berns PMJJ, Henzen-Logmans SC, Van Der Burg MEL, Alexieva-Figusch J, Klijn JGM: Prognostic value of pS2 protein and receptors for epidermal growth factor, insulin-like growth factor, and somatostatin in patients with breast and ovarian cancer. J Steroid Biochem Molec Biol 37: 815–821, 1990

4. Henry JA, Piggott NH, Mallick UK, Nicholson S, Farndon JR, Westley BR, May FEB: pNR-2/pS2 immunohistochemical staining in breast cancer: Correlation with prognostic factors and endocrine response. Br J Cancer 63: 615–622, 1991

5. Rio MC, Bellocq JP, Gairard B, Rasmussen UB, Krust A, Koehl C,

Calderoli H, Schiff V, Renaud R, Chambon P: Specific expression of the pS2 gene in subclasses of breast cancer in comparison with expression of the estrogen and progesterone receptors and the oncogene ERBB2. Proc Natl Acad Sci USA 84: 9243–9247, 1987

6. Hähnel E, Joyce R, Sterrett GF, Harvey JM, Hähnel R: Detection of estradiol-induced messenger RNA (pS2) in uninvolved breast tissue from mastectomies for breast cancer. Breast Cancer Res Treat 20: 167–176, 1991

7. Bradford M: A rapid and sensitive method for the quantitation of microgram quantities of protein utilizing the principle of protein-dye binding. Anal Biochem 72: 248–254, 1976

8. CIS ELSA-pS2: Immunoradiometric assay of pS2 protein. Package insert, December, 1990

9. Kouyoumdjian JC, Boissier B, Rymer JC, Bagnard G, Rotten D, Levaillant JP, Constancis B, Philippon C, Floury C, Thirion B: Determination of several prognostic parameters in human normal breast, benign mastopathies, and adenocarcinomas. J Tumour Marker Oncol 6: 111, 1991

Expression of the multidrug resistance-associated protein (MRP) mRNA and protein in normal peripheral blood and bone marrow haemopoietic cells.

Legrand O, Perrot JY, Tang R, Simonin G, Gurbuxani S, Zittoun R, Marie JP.

Laboratoire de Cinetique et de Cultures Cellulaires, Hotel Dieu, Paris, France.

We studied the expression of multidrug resistance-associated protein (MRP) in normal haemopoietic cells from peripheral blood and bone marrow. The MRP mRNA levels were estimated by RT/PCR and in situ hybridization (ISH) assay, and the protein levels by flow cytometry. 21 samples of peripheral blood and 21 samples of bone marrow (11 normal bone marrow donors, 10 patients in complete remission after chemotherapy for large cell lymphoma or acute myeloid leukaemia) were analysed. In peripheral blood the mean MRP mRNA level in CD3+ cells was statistically higher than in the other cells (3-fold by the methods used). The levels of MRP in CD3+ varied from one individual to another (4.5-34.8 units by RT/PCR and 5-23 grains/cell by ISH); however, this was proportional to the variation in all the cell lineages of same individual ($r = 0.84$). In bone marrow the mean MRP levels of the various cell lineages (including CD34+) were similar to the basal level in HL60 cells. Individual expression levels were again variable; however, there was no difference between untreated normal bone marrow and post chemotherapy normal bone marrow. MRP protein expression was determined by flow cytometry with the monoclonal antibody MRPm6. The CD4+ lymphocytes exhibited a higher MRP protein expression than the other cell lineages, including CD8+ cells. There was a good correlation between the three methods used (RT/PCR and ISH, $P = 0.0001$, $r = 0.87$; RT/PCR and flow cytometry, $P = 0.0001$, $r = 0.85$; ISH and flow cytometry, $P = 0.002$, $r = 0.67$).

Vascular endothelial growth factor enhances cardiac allograft arteriosclerosis.

Lemstrom KB, Krebs R, Nykanen AI, Tikkanen JM, Sihvola RK, Aaltola EM, Hayry PJ, Wood J, Alitalo K, Yla-Herttuala S, Koskinen PK.

Cardiopulmonary Research Group, Transplantation Laboratory, University of Helsinki and Helsinki University Central Hospital, Helsinki, Finland. Karl.Lemstrom@helsinki.fi

BACKGROUND: Cardiac allograft arteriosclerosis is a complex process of alloimmune response, chronic inflammation, and smooth muscle cell proliferation that includes cross talk between cytokines and growth factors. METHODS AND RESULTS: Our results in rat cardiac allografts established alloimmune response as an alternative stimulus capable of inducing vascular endothelial growth factor (VEGF) mRNA and protein expression in cardiomyocytes and graft-infiltrating mononuclear inflammatory cells, which suggests that these cells may function as a source of VEGF to the cells of coronary arteries. Linear regression analysis of these allografts with different stages of arteriosclerotic lesions revealed a strong correlation between intragraft VEGF protein expression and the development of intimal thickening, whereas blockade of signaling downstream of VEGF receptor significantly reduced arteriosclerotic lesions. In addition, in cholesterol-fed rabbits, intracoronary perfusion of cardiac allografts with a clinical-grade adenoviral vector that encoded mouse VEGF(164) enhanced the formation of arteriosclerotic lesions, possibly secondary to increased intragraft influx of macrophages and neovascularization in the intimal lesions. CONCLUSIONS: Our findings suggest a positive regulatory role between VEGF and coronary arteriosclerotic lesion formation in the allograft cytokine microenvironment.
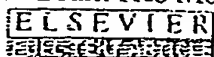
[3H]MK-801 binding and the mRNA for the NMDAR1 subunit of the NMDA receptor are differentially distributed in human and rat forebrain.

Meoni P, Mugnaini M, Bunnemann BH, Trist DG, Bowery NG.

Department of Pharmacology, Medical School, University of Birmingham, UK.
meonip@novel15.bham.ac.uk

The distributions of [3H]MK-801 binding and the NMDA NR1 subunit mRNA were studied using receptor autoradiography and in-situ hybridization in rat and human brain whole-hemisphere coronal sections. Receptor protein detected by radioligand autoradiography and the mRNA for the key subunit of the receptor presented similar distributions in the forebrain, with a few areas showing an imbalance between the levels of mRNA and receptor protein. Human frontal cortex showed a relative abundance of NMDAR1 mRNA as compared to [3H]MK-801 binding. The same area in rat brain did not show any difference in the two distributions. In comparison, the rat claustrum presented a relative excess of NMDAR1 mRNA which was not detected in human sections. Human caudate nucleus exhibited relatively high levels of [3H]MK-801 binding that were unmatched in rat caudate. The hippocampi of either species presented similar levels of [3H]MK-801 binding and NMDAR1 mRNA, but when the two signals were measured in specific subfields of the hippocampal formation, the differential distribution of the two signals reflected the anatomy of hippocampal connections assuming a preferential dendritic distribution for MK-801 binding. Interestingly, rat and human hippocampi also showed some important species-dependent difference in the relative distribution of the receptor protein and mRNA. The data presented show an overall good correlation between the mRNA for the key subunit of the NMDA receptor and the functional receptor detected with radioligand binding and highlight the presence of local differences in their ratio. This may reflect different splicing of the mRNA for the NMDAR1 subunit in specific brain areas of rat and human. The species-dependent differences in the relative distribution of the mRNA for the key subunit of the NMDA receptor and that of a marker of functional receptors also highlights important differences in the NMDA function in rat and human brain.

Differential expression of the short and long forms of the gamma 2 subunit of the GABAA/benzodiazepine receptors.

Miralles CP, Gutierrez A, Khan ZU, Vitorica J, De Blas AL.

Division of Molecular Biology and Biochemistry, School of Biological Sciences, University of Missouri-Kansas City 64110-2499.

The distribution of the mRNAs encoding the gamma 2S and gamma 2L subunits of the GABAA receptor in the rat brain has been revealed by in situ hybridization, northern blot and dot blot analysis using specific antisense oligonucleotides. In addition, the quantitative distribution of the gamma 2S and gamma 2L subunit peptides participating in the fully assembled GABAA receptors/benzodiazepine receptors has been mapped by immunoprecipitation with specific anti-gamma 2S and anti-gamma 2L antibodies. Several neuronal types and brain regions are enriched in gamma 2L such as neurons of the layer II of striate cortex and cerebellar Purkinje cells as well as the inferior colliculus, superior colliculus, deep cerebellar nuclei, medulla and pons. Other neuronal types and regions are enriched in gamma 2S such as the mitral cells of the olfactory bulb, pyramidal neurons of the pyriform cortex, layer VI of the neocortex, granule cells of the dentate gyrus and pyramidal cells of the hippocampus. Other cortical areas and cerebellar granule cells express both gamma 2S and gamma 2L in comparable amounts. There is a good correlation between the relative expression of gamma 2S and gamma 2L mRNAs and the relative presence of these protein subunits in fully assembled and mature receptors in the studied brain regions. The differential distribution of gamma 2S and gamma 2L might result in differential ethanol sensitivity of the neurons expressing these GABAA receptor subunits.

The alpha(v)beta6 integrin receptor for Foot-and-mouth disease virus is expressed constitutively on the epithelial cells targeted in cattle.

Monaghan P, Gold S, Simpson J, Zhang Z, Weinreb PH, Violette SM, Alexandersen S, Jackson T.

Institute for Animal Health, Pirbright Laboratory, Ash Road, Pirbright, Surrey GU24 0NF, UK.

Field strains of Foot-and-mouth disease virus (FMDV) use a number of alpha(v)-integrins as receptors to initiate infection on cultured cells, and integrins are believed to be the receptors used to target epithelial cells in animals. In this study, immunofluorescence confocal microscopy and real-time RT-PCR were used to investigate expression of two of the integrin receptors of FMDV, alpha(v)beta6 and alpha(v)beta3, within various epithelia targeted by this virus in cattle. These studies show that alpha(v)beta6 is expressed constitutively on the surfaces of epithelial cells at sites where infectious lesions occur during a natural infection, but not at sites where lesions are not normally formed. Expression of alpha(v)beta6 protein at these sites showed a good correlation with the relative abundance of beta6 mRNA. In contrast, alpha(v)beta3 protein was only detected at low levels on the vasculature and not on the epithelial cells of any of the tissues investigated. Together, these data suggest that in cattle, alpha(v)beta6, rather than alpha(v)beta3, serves as the major receptor that determines the tropism of FMDV for the epithelia normally targeted by this virus.

Comment in:

- J Invest Dermatol. 1994 Nov;103(5):742-4.

T-cell receptor V beta-family usage in primary cutaneous and primary nodal T-cell non-Hodgkin's lymphomas.

Preesman AH, Hu HZ, Tilanus MG, de Geus B, Schuurman HJ, Reitsma R, van Wichen DF, van Vloten WA, de Weger RA.

Department of Pathology, University Hospital Utrecht, The Netherlands.

To evaluate whether the expression of T-cell receptor (TCR) V beta families in eight cases of malignant T-cell lymphomas took place in a preferential manner, we analyzed four cases of mycosis fungoides (MF), the most common form of primary cutaneous T-cell non-Hodgkin's lymphomas (NHL), and four cases of primary nodal T-cell NHL. The usage of V beta families in T-cell populations was investigated on mRNA that was transcribed to cDNA using a C beta primer and reverse transcriptase. Subsequently, the specific usage of the families was analyzed by polymerase chain reaction (PCR) using combinations of the selected C beta-oligonucleotide primer and one of the family-specific V beta primers. Peripheral blood lymphocytes from four healthy volunteers and 1 "reactive" lymph node served as a control and expressed all 20 V beta families tested for. In T-cell lines, with restricted V beta expression, and in three patients with advanced MF, only one or two V beta families were expressed at the mRNA level. In an early MF lesion this monoclonal expression was absent: several V beta families were expressed with a weak intensity. This may indicate either a polyclonal origin of MF, or that too few monoclonal neoplastic cells were present in the tissue specimen. In the four nodal T-cell NHL, only one family could be clearly distinguished, whereas some of the other V beta families showed only a weak expression. These latter families represent the reactive T-cell component in the nodal T-cell NHL. Both in nodal T-cell NHL and in MF there was no preferential expression of a particular V beta family. There was a good correlation between PCR data and the expression of V beta-family protein products observed by immunohistochemistry on tissue sections of the T-cell lymphomas. All T-cell lines, three cases of MF, and three cases of nodal T-cell NHL showed a rearrangement of the TCR beta chain on DNA level.

ELSEVIER
FULL-TEXT ARTICLE
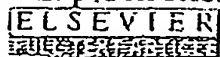
Expression and distribution of laminin alpha1 and alpha2 chains in embryonic and adult mouse tissues: an immunochemical approach.

Sasaki T, Giltay R, Talts U, Timpl R, Talts JF.

Max-Planck-Institute for Biochemistry, Martinsried, D-82152, Germany.

Protein levels, mRNA expression, and localization of laminin alpha1 and alpha2 chains in development and in adult mice were examined. Recombinant fragments were used to obtain high-titer-specific polyclonal antibodies for establishing quantitative radioimmuno-inhibition assays. This often demonstrated an abundance of alpha2 chain, but also distinct amounts of alpha1 chain for adult tissues. The highest amounts of alpha1 were found in placenta, kidney, testis, and liver and exceeded those of alpha2. All other tissue extracts showed a higher content of alpha2, which was particularly high in heart and muscle when compared to alpha1. Content of gamma1 chain, shared by most laminins, was also analyzed. This demonstrated gamma1 chain levels being equal to or moderately exceeding the sum of alpha1 and alpha2 chains, indicating that these isoforms represent the major known laminin isoforms in most adult mouse tissues so far examined. Moreover, we found good correlation between radioimmuno-inhibition data and mRNA levels of adult tissues as measured by quantitative real-time reverse transcriptase-PCR. Embryonic tissues were also analyzed by radioimmuno-inhibition assays. This demonstrated for day 11 embryos comparable amounts of alpha1 and gamma1 and a more than 25-fold lower content of alpha2. This content increased to about 10% of alpha1 in day 13 embryos. The day 18 embryo showed in heart, kidney, and liver, but not yet in brain and lung, alpha1/alpha2 chain ratios comparable to those in adult tissues. Immunostaining demonstrated alpha1 in Reichert's membrane (day 7.5), while alpha2 could not be detected before day 11.5. These data were compared with immunohistochemical localization results on several more embryonic and adult tissue sections. Our results regarding localization are consistent with those of earlier work with some notable exceptions. This was in part due to epitope masking for monoclonal antibodies commonly used in previous studies in esophagus, intestine, stomach, liver, kidney, and spleen.

Discordant regulation of granzyme H and granzyme B expression in human lymphocytes.

Sedelies KA, Sayers TJ, Edwards KM, Chen W, Pellicci DG, Godfrey DI, Trapani JA.

Cancer Immunology Laboratory, Peter MacCallum Cancer Centre, Locked Bag 1, A'Beckett Street, East Melbourne, 8006, Australia.

We analyzed the expression of granzyme H in human blood leukocytes, using a novel monoclonal antibody raised against recombinant granzyme H. 33-kDa granzyme H was easily detected in unfractionated peripheral blood mononuclear cells, due to its high constitutive expression in CD3(-)CD56(+) natural killer (NK) cells, whereas granzyme B was less abundant. The NK lymphoma cell lines, YT and Lopez, also expressed high granzyme H levels. Unstimulated CD4(+) and particularly CD8(+) T cells expressed far lower levels of granzyme H than NK cells, and various agents that classically induce T cell activation, proliferation, and enhanced granzyme B expression failed to induce granzyme H expression in T cells. Also, granzyme H was not detected in NK T cells, monocytes, or neutrophils. There was a good correlation between mRNA and protein expression in cells that synthesize both granzymes B and H, suggesting that gzmH gene transcription is regulated similarly to gzmB. Overall, our data indicate that although the gzmB and gzmH genes are tightly linked, expression of the proteins is quite discordant in T and NK cells. The finding that granzyme H is frequently more abundant than granzyme B in NK cells is consistent with a role for granzyme H in complementing the pro-apoptotic function of granzyme B in human NK cells.

Quantitative determinations of the steady state transcript levels of hexokinase isozymes and glucose transporter isoforms in normal rat tissues and the malignant tumor cell line AH130.

Shinohara Y, Yamamoto K, Inoo K, Yamazaki N, Terada H.

Faculty of Pharmaceutical Sciences, University of Tokushima, Japan.
yasuo@ph.tokushima-u.ac.jp

The steady state transcript levels of the four hexokinase (HK) isozymes and four glucose transporter (GLUT) isoforms were determined quantitatively by Northern analysis of RNA samples from rat tissues using synthetic fragments of the RNAs encoding the HK isozymes and GLUT isoforms. Results showed that the levels of HK isozyme transcripts were low in rat tissues, the level of that most highly expressed, the type I isozyme (HKI), in the brain being 0.025% of the total poly(A)+ RNA. A good correlation was found between the reported HK activities and the total amounts of transcripts encoding all HK isozymes in various tissues, showing that the HK activities in tissues can be estimated from the total amount of transcripts encoding HK isozymes. The proposed associated expressions of HK isozymes and GLUT isoforms in particular tissues were confirmed at their transcript levels. The steady state transcript levels of type II HK and the type 1 GLUT isoform in the malignant tumor cell line AH130 were also determined quantitatively.

Rat kidney glutamyl aminopeptidase (aminopeptidase A): molecular identity and cellular localization.

Song L, Ye M, Troyanovskaya M, Wilk E, Wilk S, Healy DP.

Department of Pharmacology, Mount Sinai School of Medicine, City University of New York, New York, New York 10029.

Glutamyl aminopeptidase [aminopeptidase A (EAP), EC 3.4.11.7] is an ectoenzyme that selectively hydrolyzes acidic amino acid residues from the amino terminus of oligopeptides. EAP activity is highest within the kidney and small intestine. The murine pre-B cell BP-1/6C3 and the human kidney glycoprotein gp160 differentiation antigens have been reported to have biochemical properties indistinguishable from EAP. It is not known, however, if rat kidney EAP is a homologue of these antigens or molecularly distinct. Using the reverse transcription-polymerase chain reaction method with oligonucleotide primers based on the BP-1/6C3 nucleotide sequence, we isolated a 450-bp partial cDNA from rat kidney poly(A)+ RNA. The partial cDNA encoded a predicted protein that was 92% and 86% identical to the murine BP-1/6C3 and human gp160 antigens, respectively; the amino acid sequence within the zinc-binding domain was completely conserved. Purification of EAP from rat kidney and microsequence analysis of a tryptic digest peptide fragment (18-mer) indicated that the fragment was highly similar to a region within the BP-1/6C3 and gp160 proteins. Northern blot hybridization and immunoblot analyses were also consistent with labeling of products the same size as reported for the BP-1/6C3 and gp160 antigens. There was a good correlation between the cellular distribution of EAP mRNA and EAP immunoreactivity, with proximal tubules and glomerular mesangial cells having the highest densities. These results indicate that rat kidney EAP is a species homologue of the murine BP-1/6C3 and human gp160 antigens. Furthermore, on the basis of its cellular localization, rat kidney EAP is likely to be involved in degradation of oligopeptides within the glomerulus and the glomerular filtrate. Since cells that express EAP also express receptors for angiotensin II, an intrarenal vasoactive hormone that is a substrate for EAP, these results further suggest that EAP may play a role in modulating the activity of intrarenal angiotensin II.

KARGER Full Text

Transcriptional activity of potent glucocorticoids: relevance of glucocorticoid receptor isoforms and drug metabolites.

Spika I, Hammer S, Kleuser B, Korting HC, Schafer-Korting M.

Institut fur Pharmazie, Abteilung fur Pharmakologie und Toxikologie, Freie Universitat Berlin, Berlin, Germany.

As compared to standard glucocorticoids (GC), prednicarbate (PC) is favorable in the treatment of eczema due to its high benefit/risk ratio. The remarkable anti-inflammatory effects of PC are in strong contrast to its reported low glucocorticoid receptor (GR) binding affinity. In transfected COS-7 cells we related the transcriptional potencies of PC, its metabolites and conventional GC to their receptor binding properties. Moreover, the expression pattern of the human GR isoform hGRalpha and its mutual dominant negative inhibitor hGRbeta in skin cells have been investigated as well as the influence of hGRbeta on receptor binding and transactivation. hGRalpha mRNA and protein was largely overexpressed in skin cells. hGRbeta showed no influence on hGRalpha binding and transactivation. Concentration response curves indicated the greater transactivation potency of betamethasone 17-valerate followed by dexamethasone and prednisolone 17-ethylcarbonate. Native PC appeared almost as potent as dexamethasone. With both a strong correlation was observed between transactivation and GR binding. Copyright 2003 S. Karger AG, Basel

Cell proliferation in human soft tissue tumors correlates with platelet-derived growth factor B chain expression: an immunohistochemical and in situ hybridization study.

Wang J, Coltrera MD, Gown AM.

Department of Pathology, University of Washington, Seattle 98195.

The authors tested the hypothesis that the B chain of the platelet-derived growth factor (PDGF), a known connective tissue mitogen and growth factor, could be expressed by human soft tissue tumors, and that its expression could play a role in the control of cell proliferation in these tumors. Using a set of 56 soft tissue tumors, including benign tumors and all three grades of sarcomas, PDGF-B chain protein was localized using immunohistochemistry and PDGF-B mRNA was localized using in situ hybridization. The hypothesis that PDGF-B expression was related to cell proliferation was tested by simultaneously demonstrating the expression of the proliferating cell nuclear antigen in sequential tissue sections of the same tumors. Sixty and 82% of tumors had demonstrable PDGF-B mRNA and protein, respectively, with a strong correlation between their degrees of expression ($P = 0.0001$). Among the sarcomas, a strong correlation between PDGF-B expression and increasing malignant tumor grade ($P = 0.006$), and between PDGF-B expression and increasing proliferating cell nuclear antigen index ($P = 0.01$) was found. All tumors were also demonstrated to express the beta receptor of PDGF via immunohistochemistry. These studies suggest that PDGF-B expression may be an important mediator of cell proliferation control, via an autocrine mechanism, in human soft tissue tumors and may correlate with clinical outcome in the sarcomas.

Expression of cytokines and growth factors in human glomerulonephritides.

Waldherr R, Noronha IL, Niemir Z, Kruger C, Stein H, Stumm G.

Department of Pathology, University of Heidelberg, Germany.

Numerous experimental studies point to the potential role of cytokines and growth factors in the pathogenesis of renal disease. However, from the various autocrine and paracrine mediators identified in vitro and in animal models, so far only a few have been demonstrated in selected human glomerulopathies. We examined two types of glomerulonephritis (GN): extracapillary GN with anti-neutrophil cytoplasmic autoantibodies (ANCA), an example of an acute form of GN, and mesangial IgA GN, usually a chronic form of GN, with immunocytochemistry, in situ hybridization and the polymerase chain reaction. Normal renal tissue from tumour nephrectomies served as a control. In ANCA-positive GN with active renal lesions (crescents, glomerular and vascular necrosis), infiltrating mononuclear cells in glomeruli and in the interstitium expressed interleukin (IL)-1 beta, tumour necrosis factor (TNF)-alpha, IL-2, interferon (IFN)-gamma, platelet-derived growth factor (PDGF) and transforming growth factor (TGF)-beta. Cytokine expression was also observed in activated resident cells, including endothelial cells, capsular epithelial cells, smooth muscle cells of vessel walls, fibroblasts and some tubular epithelial cells. In addition, we noted an increase in the cytokine and growth factor receptors TNF-R, IL-1R type II, IL-2R, IFN-gamma R and PDGF beta-R. In contrast, in mesangial IgA-GN, IL-1 beta, TNF-alpha, IFN-gamma and IL-2 were usually absent in glomeruli. Mesangial expansion in this disorder was accompanied by an increased expression of PDGF, PDGF beta-R, TGF-beta and IL-6 in mesangial areas. In both conditions a good correlation was observed between cytokine expression at the mRNA (in situ hybridization) and protein level (immunocytochemistry).(ABSTRACT TRUNCATED AT 250 WORDS)

Publication Types:

- Review

- Review, Tutorial

full text article of www.jpet.org

Estrogen regulation of the cytochrome P450 3A subfamily in humans.

Williams ET, Leyk M, Wrighton SA, Davies PJ, Loose DS, Shipley GL, Strobel HW.

Department of Biochemistry, Medical School, University of Texas Health Science Center at Houston, 6431 Fannin, MSB 6.200, Houston, TX 77030, USA.

This study examines the possible role of estrogen in regulating the expression of the human CYP3A subfamily: CYP3A4, CYP3A5, CYP3A7, and CYP3A43. To accomplish this goal, mRNA was quantified from human livers and endometrial samples, and total CYP3A protein levels were evaluated by Western immunoblot analysis of the liver samples. The human endometrial samples were from premenopausal and postmenopausal women. The premenopausal endometrium was either in the proliferative or secretory phase, whereas for the postmenopausal endometrium samples, the women had been treated with either a placebo or estropipate, an estrogen substitute. After analyses, CYP3A4 mRNA was shown to have lower hepatic expression in females than in males. In the endometrium, CYP3A4 and CYP3A43 are down-regulated by estrogen, whereas CYP3A5 is expressed at higher levels during the secretory phase. CYP3A7 was not detected in the endometrium. In addition, the CYP3A subfamily showed increased mRNA expression in the liver as age increased. The expression levels of total CYP3A protein and total CYP3A mRNA showed good correlation. Despite apparent regulation of CYP3A4 mRNA expression by estrogen, the effects of estrogen may be overshadowed by additional regulators of gene expression.

Expression of superoxide dismutases, catalase, and glutathione peroxidase in glioma cells.

Zhong W, Yan T, Lim R, Oberley LW.

Radiation Research Laboratory, Department of Radiology, The University of Iowa, Iowa City 52242, USA.

Four primary antioxidant enzymes were measured in both human and rat glioma cells. Both manganese-containing superoxide dismutase (MnSOD) and copper-zinc-containing superoxide dismutase (CuZnSOD) activities varied greatly among the different glioma cell lines. MnSOD was generally higher in human glioma cells than in rat glioma cells and relatively higher than in other tumor types. High levels of MnSOD in human glioma cells were due to the high levels of expression of MnSOD mRNA and protein. Heterogeneous expression of MnSOD was present in individual glioma cell lines and may be due to subpopulations or cells at different differentiation stages. Less difference in CuZnSOD, catalase, or glutathione peroxide was found between human and rat glioma cells. The human glioma cell lines showed large differences in sensitivity to the glutathione modulating drugs 1,3-bis (2-chloroethyl)-1-nitrosourea (BCNU) and buthionine sulfoximine (BSO). A good correlation was found between sensitivity to BCNU and the activities of catalase in these cell lines. Only one cell line was sensitive to BSO and this line had low CuZnSOD activity.

SpringerLink
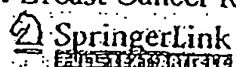
Somatostatin receptors in primary human breast cancer: quantitative analysis of mRNA for subtypes 1--5 and correlation with receptor protein expression and tumor pathology.

Kumar U, Grigorakis SI, Watt HL, Sasi R, Snell L, Watson P, Chaudhari S.

Fraser Laboratories For Diabetes Research, Department of Medicine, McGill University, Royal Victoria Hospital, 687 Pine Avenue West, H3A 1A1 Montreal, Quebec, Canada. ujendra.kumar@muhc.mcgill.ca

Somatostatin receptors (SSTRs) have been identified in most hormone-producing tumors as well as in breast cancer. In the present study, we determined SSTR1-5 expression in primary ductal NOS breast tumors through semi-quantitative RT-PCR and immunocytochemistry. The results from the analysis of 98 samples were correlated with several key histological markers and receptor expression. All five SSTR subtypes are variably expressed at the mRNA level in breast tumors with 91% of samples showing SSTR1, 98% SSTR2, 96% SSTR3, 76% SSTR4, and 54% SSTR5. SSTR1-5 are localized to both tumor cells and the surrounding peritumoral regions as detected by immunocytochemistry. Levels of SSTR mRNA, when corrected for beta-actin levels, were highest for SSTR3 followed by SSTR1, SSTR2, SSTR5, and SSTR4. Furthermore, there was good correlation between mRNA and protein expression with 84% for SSTR1, 79% for SSTR2, 89% for SSTR3, 68% for SSTR4, 68% for SSTR5, and 78% for all five receptors. SSTR1, 2 and 4 were correlated with ER levels whereas SSTR2 showed an additional correlation with PR levels. These correlations were independent of patient age and histological grade. Moreover, using immunocytochemistry, blood vessels exhibited receptor-specific localization for SSTR2 and SSTR5. Our results indicate significant correlations between mRNA and protein expression along with receptor-specific correlations with histological markers as well as ER and PR levels. Differential distribution of SSTR subtypes in tumors and receptor-specific expression in vascular structures may be considered as a novel diagnosis for breast tumors with receptor subtype agonists.
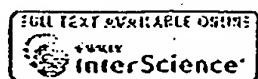
Publication Types:

- Evaluation Studies

Erratum in:

- Int J Cancer 2002 Feb 20;97(6):878.

FULL TEXT AVAILABLE ONLINE
Wiley InterScience

Immunohistochemical analysis of NY-ESO-1 antigen expression in normal and malignant human tissues.

Jungbluth AA, Chen YT, Stockert E, Busam KJ, Kolb D, Iversen K, Coplan K, Williamson B, Altorki N, Old LJ.

Ludwig Institute for Cancer Research, Memorial Sloan-Kettering Cancer Center, New York, NY, USA. jungblua@mskcc.org

NY-ESO-1, a member of the CT (cancer/testis) family of antigens, is expressed in normal testis and in a range of human tumor types. Knowledge of NY-ESO-1 expression has depended on RT-PCR detection of mRNA and there is a need for detecting NY-ESO-1 at the protein level. In the present study, a method for the immunochemical detection of NY-ESO-1 in paraffin-embedded tissues has been developed and used to define the expression pattern of NY-ESO-1 in normal tissues and in a panel of human tumors. No normal tissue other than testis showed NY-ESO-1 reactivity, and expression in testis was restricted to germ cells particularly spermatogonia. In human tumors, the frequency of NY-ESO-1 antigen expression corresponds with past analysis of NY-ESO-1 mRNA expression e.g., 20-30% of lung cancers, bladder cancers and melanoma, and no expression in colon and renal cancer. Co-typing of NY-ESO-1 antigen and mRNA expression in a large panel of lung cancers showed a good correlation. There is great variability in NY-ESO-1 expression in individual tumors, ranging from an infrequent homogeneous pattern of staining to highly heterogeneous antigen expression. Copyright 2001 Wiley-Liss, Inc.

Modulation of glucagon receptor expression and response in transfected human embryonic kidney cells.

Ikegami T, Cypess AM, Bouscarel B.

Department of Medicine, George Washington University Medical Center, Washington, District of Columbia 20037, USA.

The modulation of glucagon receptor (GR) expression and biological response was investigated in human embryonic kidney cell (HEK-293) clones permanently expressing the GR with different densities. The GR mRNA expression level in these clones was upregulated by cellular cAMP accumulation and presented a good correlation with both the protein expression level and the maximum number of glucagon binding sites. However, the determination of glucagon-induced cAMP accumulation in these cell lines revealed that the enhancement of receptor expression did not lead to a proportional increase in cAMP formation. Under these conditions, the maximum cAMP production induced by NaF and forskolin was not significantly different among selected clones, regardless of the receptor expression level. High receptor-expressing clones showed the greatest susceptibility for agonist-induced desensitization compared with clones with lower GR expression levels. The results of the present study suggest that the GR can recruit non-GR-specific desensitization mechanism(s). Furthermore, the partial inhibition or alteration of the overall cAMP synthesis pathway at the receptor level may be a necessary adaptive step for a cell in response to a massive increase in membrane receptor expression level.

This Page is Inserted by IFW Indexing and Scanning Operations and is not part of the Official Record

BEST AVAILABLE IMAGES

Defective images within this document are accurate representations of the original documents submitted by the applicant.

Defects in the images include but are not limited to the items checked:

☑ **BLACK BORDERS**

☐ **IMAGE CUT OFF AT TOP, BOTTOM OR SIDES**

☐ **FADED TEXT OR DRAWING**

☐ **BLURRED OR ILLEGIBLE TEXT OR DRAWING**

☐ **SKEWED/SLANTED IMAGES**

☐ **COLOR OR BLACK AND WHITE PHOTOGRAPHS**

☐ **GRAY SCALE DOCUMENTS**

☑ **LINES OR MARKS ON ORIGINAL DOCUMENT**

☑ **REFERENCE(S) OR EXHIBIT(S) SUBMITTED ARE POOR QUALITY**

☐ **OTHER:** _____

IMAGES ARE BEST AVAILABLE COPY.
As rescanning these documents will not correct the image problems checked, please do not report these problems to the IFW Image Problem Mailbox.